



Evolutionary shaping of low-dimensional path facilitates robust and plastic switching between phenotypes

Ayaka Sakata ^{1,2,*} and Kunihiko Kaneko ^{3,4}

¹Department of Statistical Inference & Mathematics, The Institute of Statistical Mathematics, Tachikawa, Tokyo 190-8562, Japan

²Department of Statistical Science, The Graduate University for Advanced Science (SOKENDAI), Hayama-cho, Kanagawa 240-0193, Japan

³Center for Complex Systems Biology, Universal Biology Institute, University of Tokyo, Komaba, Tokyo 153-8902, Japan

⁴The Niels Bohr Institute, University of Copenhagen, Blegdamsvej 17, Copenhagen 2100-DK, Denmark



(Received 22 April 2023; accepted 6 October 2023; published 26 December 2023; corrected 8 February 2024)

Biological systems must be robust for stable functioning against perturbations, but robustness alone is insufficient. The ability to switch between appropriate states (phenotypes) in response to different conditions is essential for biological functions, as observed in allosteric enzymes and motor proteins. How are robustness and plasticity simultaneously acquired through evolution? In an attempt to answer this question, we examine the evolution of genotypes that realize plastic switching between two endpoint phenotypes upon external inputs as well as stationary expressions of phenotypes. Here, we introduce a statistical physics model consisting of spins, with active sites and regulatory sites, which are distinct from each other. In our model, we represent the phenotype and genotype as spin configurations and spin-spin interactions, respectively. The fitness for selection is given by the spin configuration, whose behavior is governed by the genotypes. Specifically, the fitness for selection is given so that it takes a higher value as more active sites take two requested spin configurations depending on the states of the regulatory sites. The remaining spins do not directly affect the fitness, but they interact with other spins. We numerically evolve the matrices of spin-spin interactions (genotypes) by changing them with mutations and selection of those with higher fitness. Our numerical simulations show that characteristic genotypes with higher fitness evolve slightly above the phase transition temperature between replica-symmetric and replica-symmetry-breaking phase in spin-glass theory. These genotypes shape the two spin configurations separately depending on the regulation. Each phenotype is primarily represented by the first or second eigenmode of the genotypes. Smooth switching between the two phenotypes is achieved by following a one-dimensional quarter-circle that connects them. Upon changes in regulations, spin configurations are attracted to this path, which allows for robust and plastic switching between the two phenotypes. The statistical physics analysis based on the two eigenmodes shows that the free energy landscape has a valley along the one-dimensional quarter-circle switching path. Robust attraction to the path is achieved through the evolution of the interactions within nonactive and nonregulatory spin sites, which themselves do not contribute to fitness. Our findings indicate that the compatibility between robustness and plasticity is acquired by the evolution of low dimensionality in the phenotype space, which will be relevant to the understanding of the robust function of protein as well as material design.

DOI: [10.1103/PhysRevResearch.5.043296](https://doi.org/10.1103/PhysRevResearch.5.043296)

I. INTRODUCTION

Biological systems are inherently complex and comprise numerous elements. Despite such complexity, they function robustly under environmental and stochastic perturbations. In general, the biological functions are determined by phenotypes, which are generated through expression dynamics based on genetic information. Hence, function-related phenotypes need to be robustly shaped through the dynamics.

However, a single robust phenotype or fitted state is insufficient for a biological system to function under varying conditions. Phenotypes must exhibit plasticity, shifting to appropriate patterns in response to relevant signals or inputs [1,2]. For instance, the active sites of enzymes can change between two conformations known as tense and relaxed states, induced by allosteric regulation [3–6]. Motor proteins, such as those belonging to the myosin, kinesin, and dynein families, exhibit large-scale conformational changes in response to binding events [7,8]. Phosphorylation of substrates in the mitogen-activated protein kinase cascades can switch between two states depending on modification by phosphatase or diphosphatase [9]. Switches in gene expression pattern in response to signals are also necessary for cell survival. Thus, the ability to switch between appropriate phenotypes in response to different conditions is essential for biological functions. Accordingly, the presence of multiple phenotypes

*ayaka@ism.ac.jp

Published by the American Physical Society under the terms of the [Creative Commons Attribution 4.0 International](https://creativecommons.org/licenses/by/4.0/) license. Further distribution of this work must maintain attribution to the author(s) and the published article's title, journal citation, and DOI.

and transitions among them in response to inputs must be shaped through evolution. Considering such changes in the phenotype, plasticity to external conditions is also required for switching to different phenotypes, in addition to the robust expression of each phenotype. In general, the compatibility between robustness and plasticity remains a fundamental question in biology [10,11].

To study such plastic responses in biological systems, it is essential to understand the nature of switching pathways, in addition to the multiple phenotypes corresponding to endpoint structures. An understanding of the switching pathways can aid in the development of engineering techniques, such as drug design, that target the intermediate states of the switching pathways [12,13]. Despite advances in structural biology in recent decades, molecular-level characterization of switching remains a challenge owing to limitations in macromolecular x-ray crystallography, nuclear magnetic resonance, and small-angle x-ray scattering [14]. Hence, theoretical or numerical approaches are necessary to understand general characteristics of large-scale conformational switching [15,16]. For instance, the plastic network model, an extension of the elastic network model [17–19], has been utilized to generate conformational switching pathways that are consistent with experimental data of the intermediate structures in *Escherichia coli* adenylate kinase [7]. The resulting pathways resemble combinations of low-energy normal modes obtained for the endpoint structures [7]. It has also been suggested that such preferred directionality may contribute to catalysis in many enzymes, achieving extraordinary rate acceleration and specificity [20]. Such switching paths were explored for Src kinase, by using a coarse-grained, two-state Go model, characterized by a two-dimensional free energy landscape [21].

In general, theoretical and numerical methods to explore conformational changes assume the existence of probable switching paths, which minimize energy, free energy, or action [22]. The existence of a probable path implies that possible transient changes are constrained along the path. Further, low-dimensional approximations using principle component analysis have often been adopted to simplify the numerically or experimentally obtained switching paths [16]. These above-mentioned studies suggest the importance of understanding how low-dimensional switching paths have shaped and evolved in the phenotypic spaces.

As for the stationary states, recent experimental and numerical observations have shown that evolved phenotypes are often constrained within a low-dimensional manifold despite the high dimensionality of the phenotypic space. For example, changes in (logarithmic) concentrations of mRNAs or proteins have been found to be correlated [23–26] or proportional [27,28] across all components under various environmental stresses. Numerical simulations of cell models with catalytic reaction networks have also demonstrated that evolved phenotypic changes caused by environmental and mutational changes are constrained within a low-dimensional manifold [29]. This reduction in dimensionality from high-dimensional phenotypes has also been observed during the structural changes of proteins via data analysis [30]. Additionally, such dimensional reduction is suggested to be a result of the robustness of phenotypes shaped by evolution. However, such studies are limited to phenotypes around the endpoint

structures, i.e., the stationary conditions. In this paper, we examine the evolution of the switching path from the viewpoint of dimensional reduction.

We address the following questions:

- (1) Under what conditions and how are multiple endpoint phenotypes shaped depending upon external inputs and stabilized through evolution?
- (2) Are low-dimensional constraints of switching paths shaped through evolution?
- (3) What are the characteristics of switching paths between endpoints?
- (4) What are the characteristics of evolved genotypes that allow robust switching paths?

To address these questions, we extend a spin-statistical physics model introduced previously [31]. In this model, the spin variables \mathbf{S} and their interaction variables \mathbf{J} represent phenotype and genotype [32–34], respectively, and fitness is provided by certain spin configurations. We consider two endpoint structures, corresponding to those under regulation and without regulation. We introduce active and regulatory sites in the spin system to represent the effect of external regulation applied to the regulatory sites. The fitness of selective evolution depends on the appropriate expression of configurations. Fitted interactions can provide two configurations of active spins, corresponding to regulated and nonregulated cases.

Numerical evolution allows us to examine how the robustness of each phenotype, as well as its plasticity to switch between the two configurations, is shaped by regulation. Our results show that, as a result of evolution, the dimensional reduction to a two-dimensional phenotypic space appears under a certain range of temperatures, while a one-dimensional path is shaped for the switch between two phenotypes in the regulated and nonregulated cases. The shaped switching path is robust to thermal noise and genetic mutation. In terms of statistical physics, the robustness of the fitted phenotype is achieved in the replica-symmetric phase. In contrast, the plasticity of the switch increases as the temperature approaches the replica-symmetry-breaking (RSB) transition. We then demonstrate that robust response is achieved near the RSB transition.

II. MODEL

Here, we introduce an abstract model of interacting spins, as a simplified representation of proteins whose active site conformation is regulated via regulatory sites. Fig. 1(a) is a simplified picture of the regulation and related conformational changes adopted in this paper. The protein shown in gray in the figure has an active site (A) and a regulatory site (R), which consist of amino-acid residues. In general allosteric regulation, the active and regulatory sites are located sufficiently apart and do not interact directly. As shown in Fig. 1(a), binding of the ligand to the regulatory site leads to a conformational change in the active site, via interaction with sites other than the active and regulatory sites. In contrast, without the binding of the activator to the regulatory site, such conformational changes in the active site do not occur, and the protein remains in its original conformation.

Here, we introduce an abstract statistical physics model with interacting spins representing conformation, as shown

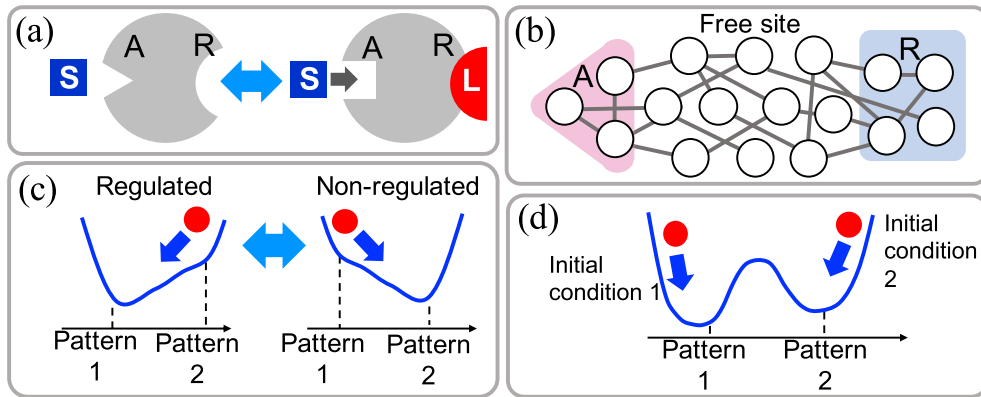


FIG. 1. (a) Schematic representation of the conformational change induced by regulation. A, R, and S denote active sites, regulatory sites, and substrates, respectively. The molecule denoted by L is the ligand that regulates the protein through regulatory sites. (b) The spin model for conformational switching that has active and regulatory sites. (c) A landscape picture of the conformational changes induced by regulations discussed in this paper. (d) Free energy landscape of the multipattern embedding in the associative memory model such as Hopfield networks.

in Fig. 1(b). The model consists of spin variable $\mathbf{S} = \{S_1, \dots, S_N\} \in \{-1, +1\}^N$, which represents the conformational change in each amino-acid residue, whereas the coupling \mathbf{J} between spins represents the interaction among residues. These are denoted by nodes and edges, respectively, in Fig. 1(b). Here, we set \mathbf{J} as the $N \times N$ symmetric matrix. Its elements are given by $J_{ii} = 0$ ($i = 1, \dots, N$), and $J_{ij} \in \Omega_J$ for $i \neq j$, where $\Omega_J = \{-1/\sqrt{N}, 0, 1/\sqrt{N}\}$. Active (A) and regulatory (R) sites are represented by N_A and N_R spins, respectively, among the N spins. The label sets of active and regulatory spins are denoted by \mathcal{A} and \mathcal{R} , respectively. We set $J_{ij} = 0$ for $i \in \mathcal{A}$ and $j \in \mathcal{R}$ or $i \in \mathcal{R}$ and $j \in \mathcal{A}$ to prohibit direct interaction between the regulatory and active sites. The spin variables other than those at the active and regulatory sites are called free sites, as shown in Fig. 1(b).

For the dynamics of spin variables under given \mathbf{J} , we adopt the transition rule of spins from \mathbf{S} to \mathbf{S}' under the given Hamiltonian with the interaction matrix \mathbf{J} and temperature T as

$$\Pr[\mathbf{S} \rightarrow \mathbf{S}' | \mathbf{J}] = \min\{\exp[-\beta \Delta_H(\mathbf{S}, \mathbf{S}' | \mathbf{J})], 1\}, \quad (1)$$

where $\beta = T^{-1}$ is the inverse of temperature, and $\Delta_H(\mathbf{S}, \mathbf{S}' | \mathbf{J}) \equiv H(\mathbf{S}' | \mathbf{J}) - H(\mathbf{S} | \mathbf{J})$. The candidate spin configuration \mathbf{S}' is generated by randomly changing the state of a single site from \mathbf{S} . Here, we set the Hamiltonian as

$$H(\mathbf{S} | \mathbf{J}) = - \sum_{i < j} J_{ij} S_i S_j. \quad (2)$$

Note that, in this statistical physics model, we adopt the spin variables $\{-1, 1\}$, instead of continuous conformational variables in the residues. This is a highly simplified model (see Ref. [35] for examples of spin models for protein dynamics). Here, we aim to elucidate how certain stochastic dynamics for generating functional phenotypes are shaped through evolution. Nevertheless, the present model captures the essence of such dynamics and genotype-phenotype mapping, in which spin variables \mathbf{S} corresponding to the phenotypes are shaped by high-dimensional dynamics under genetic rules given by the interaction matrix \mathbf{J} , whereas regulation is referred to as change in a part of regulatory spins, as defined below.

The functional change in the active sites is postulated by an appropriate change in the configuration of active spins $\mathbf{S}_{\mathcal{A}} = \{S_i | i \in \mathcal{A}\}$, depending on the configurations of the regulatory site $\mathbf{S}_{\mathcal{R}} = \{S_i | i \in \mathcal{R}\}$. Here, instead of introducing the binding of ligands to regulatory sites as external variables, we assume that the configuration of the spins is set at $\mathbf{S}_{\mathcal{R}}^+$ upon the binding. That is, among 2^{N_R} possible configurations of the regulatory spins, the regulatory spins only take the configuration in $\mathbf{S}_{\mathcal{R}}^+$ when the ligand binding occurs. Further, we consider that $\mathbf{S}_{\mathcal{R}}^+$ cannot appear without the ligand binding. Accordingly, the equilibrium distribution upon regulation and nonregulation is given by

$$P_{\beta}^+(\mathbf{S} | \mathbf{J}) = \frac{1}{Z_{\beta}^+} \exp[-\beta H(\mathbf{S} | \mathbf{J})],$$

$$Z_{\beta}^+(\mathbf{J}) = \sum_{\mathbf{S} | \mathbf{S}_{\mathcal{R}} \in \mathbf{S}_{\mathcal{R}}^+} \exp(-\beta H), \quad (3)$$

$$P_{\beta}^-(\mathbf{S} | \mathbf{J}) = \frac{1}{Z_{\beta}^-} \exp[-\beta H(\mathbf{S} | \mathbf{J})],$$

$$Z_{\beta}^-(\mathbf{J}) = \sum_{\mathbf{S} | \mathbf{S}_{\mathcal{R}} \notin \mathbf{S}_{\mathcal{R}}^+} \exp(-\beta H), \quad (4)$$

where $\mathbf{S} | \mathbf{S}_{\mathcal{R}} \in \mathbf{S}_{\mathcal{R}}^+$ and $\mathbf{S} | \mathbf{S}_{\mathcal{R}} \notin \mathbf{S}_{\mathcal{R}}^+$ indicate the set of possible configurations for regulated and nonregulated states, respectively.

The functional change in configurations of the active spins in response to the regulation is given by the change in regulatory spins from $\mathbf{S}_{\mathcal{R}}^-$ to $\mathbf{S}_{\mathcal{R}}^+$. Thus, the conformational change induced by regulation is modeled as follows: If the configuration of regulatory spins is set at $\mathbf{S}_{\mathcal{R}}^+$, the configuration of the active spins turns into $\mathbf{S}_{\mathcal{A}}^+$; else, the configuration of the active sites stays at $\mathbf{S}_{\mathcal{A}}^-$.

The function of the present system to express the target spin pattern $\mathbf{S}_{\mathcal{A}}^{\pm}$ appropriately can be measured by magnetization $m_{\mathcal{A}}^{\pm}$, defined as the overlap of the spins in the active sites

with the corresponding target spin patterns as

$$m_A^+ = \frac{1}{N_A} \sum_{i \in \mathcal{A}} S_i S_i^+, \quad (5)$$

$$m_A^- = \frac{1}{N_A} \sum_{i \in \mathcal{A}} S_i S_i^-. \quad (6)$$

Finally, the overall fitness that measures the functionality of the present system is given by the sum of the expectations of m_A^\pm as

$$\psi(\mathbf{J}) = \frac{1}{2} \{ \langle |m_A^+| \rangle_+ + \langle |m_A^-| \rangle_- \}, \quad (7)$$

where $\langle \cdot \rangle_+$ and $\langle \cdot \rangle_-$ are the expectation values according to the equilibrium distributions for regulated and nonregulated cases in Eqs. (3) and (4),

The evolution of genotypes \mathbf{J} is then based on the above fitness $\psi(\mathbf{J})$. Genotypes with higher fitness are selected under given selection pressure: At generation g , the evolutionary change in \mathbf{J} to increase the fitness is given by

$$\text{Pr}[\mathbf{J}^{(g)} \rightarrow \mathbf{J}^{(g+1)}] = \min\{\exp(\beta_J \Delta\psi), 1\}, \quad (8)$$

where $\Delta\psi = \psi[\mathbf{J}^{(g+1)}] - \psi[\mathbf{J}^{(g)}]$. The parameter $\beta_J = T_J^{-1}$ expresses the selection pressure, and the genotypes are selected uniformly at high temperatures $T_J \rightarrow \infty$, whereas at low T_J , genotypes with higher fitness values are preferred [36].

Remark: The celebrated Hopfield neural network model can be used for embedding several patterns in spin models [37]. In this case, as schematically shown in Fig. 1(d), multiple patterns with different spin configurations were reached depending on the initial condition given by Hamiltonian dynamics. In contrast, in this paper, different spin configurations were reached depending on whether the system is regulated or not by external inputs to regulatory spins (i.e., with inputs or with different boundary conditions) from the same initial conditions for the two, as in Fig. 1(c), a picture which has been introduced in the study of the reshaping of the energy landscape of a protein by allostery [38]. (In the context of the neural network model, this corresponds to the associative memory model upon external inputs [39].)

III. NUMERICAL SIMULATION

Without loss of generality, we set the indices of the regulatory sites and active sites as $\mathcal{R} = \{N - N_R + 1, \dots, N\}$ and $\mathcal{A} = \{1, \dots, N_A\}$, respectively. Further, we set the configuration $\mathbf{S}_{\mathcal{R}}^+$ as $\mathbf{S}_{\mathcal{R}}^+ = \{ \{+1, \dots, +1\}, \{-1, \dots, -1\} \}$. For the desirable configurations of the active sites, we set $\mathbf{S}_{\mathcal{A}}^+ = \{ \{+1, \dots, +1\}, \{-1, \dots, -1\} \}$ and $\mathbf{S}_{\mathcal{A}}^- = \{ \{+1, -1, \dots\}, \{-1, +1, \dots\} \}$. In the genotype evolution process, we induce a 10-point mutation at each generation to generate the candidate of the next-generation \mathbf{J}' from \mathbf{J} , maintaining the symmetry $\mathbf{J}'^T = \mathbf{J}'$. We focus on the equilibrium properties of the ensemble of genotypes after sufficient generations. Under the evolutionary rule in Eq. (8), the ensemble is expected to be characterized by the distribution $\propto \exp(\beta_J \Psi)$ without depending on the details of the mutation. Here, we mainly show the results for $N = 100$, $N_A = 5$, and $N_R = 10$, and the free sites consist of $N - N_A - N_R = 85$ spin variables.

We update \mathbf{J} at a sufficiently large value as $\beta_J = 100$ and discuss T dependencies.

A. Fitness, rugged landscape, and separation of two patterns

In Fig. 2, we show examples of evolutionary dynamics of \mathbf{J} through the evolutionary changes of $\langle |m_A^\pm| \rangle_\pm^{(g)}$, where $\langle \cdot \rangle^{(g)}$ denotes expectation according to distribution $P_\beta^\pm[\mathbf{S}|\mathbf{J}^{(g)}]$ with a g th-generation genotype $\mathbf{J}^{(g)}$. These quantities measure the tendency to exhibit desirable patterns depending on the regulatory site, whereas fitness is given by their mean, as in Eq. (7). Figure 2(a) shows an example of the generational changes of $\langle |m_A^\pm| \rangle_\pm^{(g)}$ at $T = 0.91$. They show a negative correlation, i.e., when $\langle |m_A^+| \rangle_+^{(g)}$ increases, $\langle |m_A^-| \rangle_-^{(g)}$ decreases, and vice versa. For genotypes that show such behavior, which are the most evolved genotypes around $T = 0.91$, the simultaneous expression of $\mathbf{S}_{\mathcal{A}}^+$ and $\mathbf{S}_{\mathcal{A}}^-$, depending on the regulatory sites, is difficult. When the active sites take one of the configurations in $\mathbf{S}_{\mathcal{A}}^+$ or $\mathbf{S}_{\mathcal{A}}^-$, irrespective of the regulatory sites, we obtain $|m_A^+| = 1$ and $|m_A^-| = 0.2$ or $|m_A^+| = 0.2$ and $|m_A^-| = 1$, respectively. Therefore, the fitness value of the genotype that can express only one desirable pattern among $\mathbf{S}_{\mathcal{A}}^\pm$ can achieve a maximum value of 0.6. Meanwhile, at a lower temperature $T = 0.67$, both $\langle |m_A^\pm| \rangle_\pm^{(g)}$ increase simultaneously after evolution, as shown in Figs. 2(b)–2(d), and the fitness value reaches ~ 0.9 . There are three evolutionary courses; $\langle |m_A^+| \rangle_+^{(g)}$ or $\langle |m_A^-| \rangle_-^{(g)}$ increases first [Fig. 2(b) or 2(c)], or they increase simultaneously [Fig. 2(d)]. Among the 100 samples, 21, 33, and 46 samples follow each course, respectively.

For each T , we obtain 100 samples of the evolved \mathbf{J} updated for $g = 10^5$ generations and denote the temperature-dependence ensemble of evolved genotypes as $\mathcal{J}(T)$. Figure 3(a) shows the T dependence of the mean of the fitness among $\mathcal{J}(T)$. With a decrease in T , the fitness value Ψ increases from 0.4, which is a trivial value given by the uniform distribution of the phenotype \mathbf{S} . Here, T_0 is defined as the transition temperature characterized by fitness, below which the fitness value increases as T decreases. To be precise, it is defined by the point where the derivative of Ψ shows a large change that corresponds to the singularity at the thermodynamic limit. We term the phase $T > T_0$ as the paramagnetic phase. Next, the energy landscape on $\mathbf{J} \in \mathcal{J}(T)$, which governs the dynamics of phenotype expression, exhibits significant differences between $T < T_2$ and $T > T_2$: We term the phases at $T_0 > T > T_2$ and $T < T_2$ as the replica-symmetric (RS) and RSB phases, respectively. The difference between the two phases can be detected by the belief propagation (BP) algorithm [40–42]. In a fully connected spin-glass system, the stability of the BP algorithm agrees with the validity of the RS assumption in the replica analysis, which is known as de Almeida–Thouless (AT) instability [43,44]. Hence, when the BP algorithm converges, the system on \mathbf{J} corresponds to the RS phase; otherwise, it corresponds to the RSB phase. The RSB phase indicates the rugged landscape with exponential orders of metastable states, and the phenotype expression dynamics is not robust to thermal fluctuation [32,45]. At $T > T_2$, most of the evolved genotypes in $\mathcal{J}(T)$ exhibit rapid convergence of the BP algorithm. Meanwhile, the BP algorithm cannot converge for highly evolved

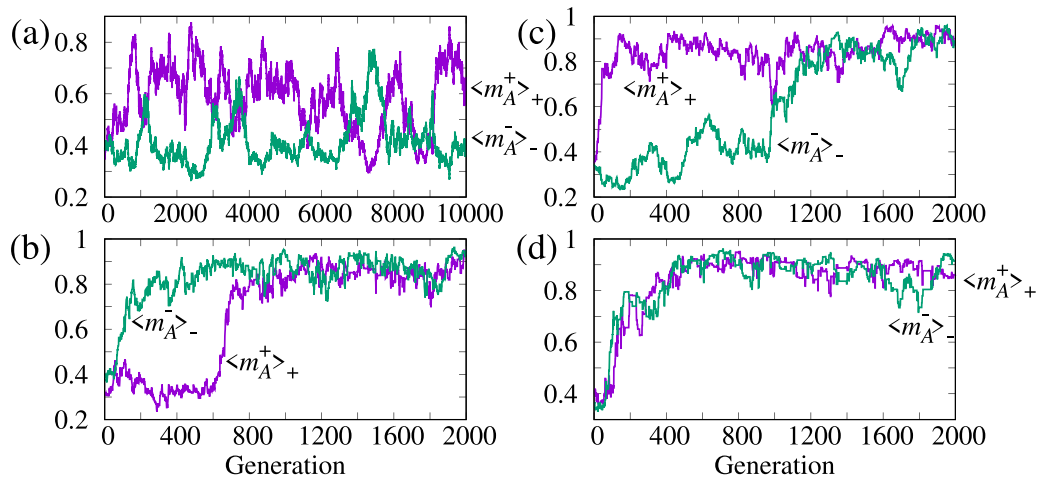


FIG. 2. Evolutional dynamics of $\langle m_A^\pm \rangle$ associated with the evolution of a genotype \mathbf{J} . An example at $T = 0.91$ is shown in (a), and examples at $T = 0.67$ are shown in (b)–(d).

genotypes in $\mathcal{J}(T)$ when $T < T_2$. In Fig. 3(b), we present the fraction of evolved genotypes for which the BP algorithm does not appear to converge within 10^5 steps, which increases as T is decreased below T_2 .

The existence of these transitions from the paramagnetic phase to the RS phase and then to the RSB phase is common with the evolving spin-glass model to express one specific phenotype [31–34]. In the present model, however, another transition appears at T_1 , with respect to the achievability of two patterns. In Fig. 3(c), we show the temperature dependence of the overlaps $\langle |m_A^+| \rangle_+$ and $\langle |m_A^-| \rangle_-$, whose mean corresponds to fitness. At $T_1 < T < T_0$, $\langle |m_A^+| \rangle_+$ contributes more to fitness, and only the phenotype expression with regulation is preferentially shaped. However, at $T < T_1$, both the increase of $\langle |m_A^+| \rangle_+$ and $\langle |m_A^-| \rangle_-$ are achieved depending on the regulatory site. We term the phases $T_0 > T > T_1$ and $T_1 > T > T_2$ as RS1 and RS2, respectively. Here, we note

a negative correlation between $\langle m_A^+ \rangle_+^{(g)}$ and $\langle m_A^- \rangle_-^{(g)}$ in the paramagnetic and RS1 phases, as shown in Fig. 2(a). At temperature T_1 , the phenotypes for dominant genotypes distinctly change, as is presented later. In the RS2 and RSB phases, the increase of both $\langle m_A^+ \rangle_+^{(g)}$ and $\langle m_A^- \rangle_-^{(g)}$ is achieved after a sufficient update, as shown in Figs. 2(b)–2(d).

To study the transition at $T = T_1$, we examined the probability distributions of spin configurations, $p_\beta^+(\mathbf{S}|\mathbf{J})$ and $p_\beta^-(\mathbf{S}|\mathbf{J})$, with and without regulations, by means of the component-wise expected phenotype for each $i = 1, \dots, N$, which is defined as

$$\mu_i^\pm = \left\langle \text{sign} \left(\sum_{i=1}^{N_A} S_i \right) S_i \right\rangle_\pm, \quad (9)$$

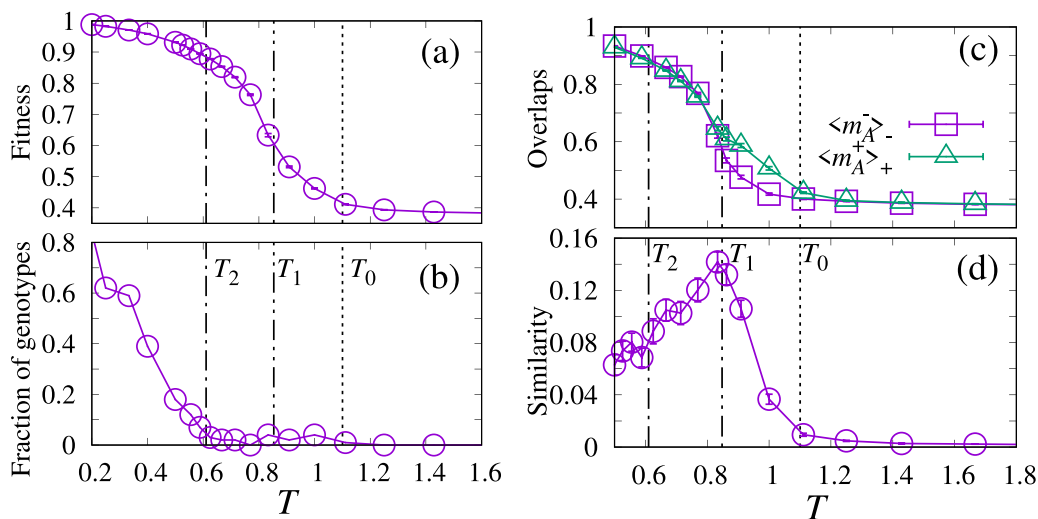


FIG. 3. T dependence of (a) fitness, (b) the fraction of genotypes on which the belief propagation (BP) algorithm does not converge, (c) $\langle m_A^+ \rangle_+$ and $\langle m_A^- \rangle_-$, and (d) similarity between regulated and nonregulated states. Each data point is averaged over 100 samples of evolved \mathbf{J} . The vertical dotted line, two-dot chain line, and one-dot chain line denote T_0 , T_1 , and T_2 , respectively.

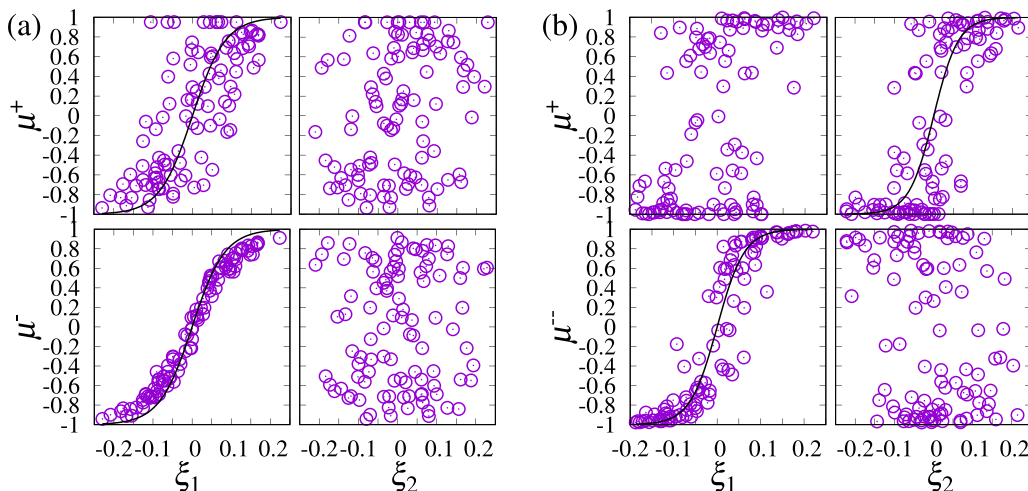


FIG. 4. Comparison between the eigenvectors (ξ_1 and ξ_2) and μ^\pm for one sample of evolved $\mathbf{J} \in \mathcal{J}(T)$ at (a) $T = 0.833$ and (b) $T = 0.667$. The solid lines show the relationship $y = \tanh(\beta\sqrt{N}x)$.

where the term $\text{sign}(\sum_{i=1}^{N_A} S_i)$ is introduced to break the Z2 symmetry. In Fig. 3(d), we show T dependence of the similarities between the two mean phenotypes measured by $\sum_{i=1}^N \mu_i^+ \mu_i^- / N$. As shown in Fig. 3(d), the overlap shows a peak at $T = T_1$, and it decreases as T decreases below T_1 . According to the decrease in the overlap, the transition between the phenotype with and without regulation involves large conformational changes.

B. Two-dimensional structure in the phenotype space

We investigated how the two patterns shaped by evolution are separated in the RS2 phase. To compare N -dimensional mean phenotypes μ^+ under and μ^- without regulation, it is convenient to determine a reference coordinate system. We adopted the eigenvectors of the evolved genotypes as the axes to represent mean phenotypes. Using the eigenvectors and corresponding eigenvalues, the genotype \mathbf{J} is expressed as

$$\mathbf{J} = \sum_{r=1}^N \lambda_r \xi_r \xi_r^\top, \quad (10)$$

where ξ_i and λ_i are the i th eigenvector and i th eigenvalue. We set the indices of the eigenmodes to be $\lambda_1 \geq \lambda_2 \geq \dots \geq \lambda_N$.

In Fig. 4, we show the scatter plots between μ_i^\pm against eigenvectors ξ_{1i} and ξ_{2i} for $i = 1, \dots, N$ at (a) $T = 0.833$ (RS1 phase) and (b) $T = 0.667$ (RS2 phase) under one realization of $\mathbf{J} \in \mathcal{J}(T)$. In the RS1 phase, the mean phenotypes μ^\pm and particularly μ^- are highly correlated with ξ_1 , as described by $y = \tanh(\beta\sqrt{N}x)$ [see Fig. 4(a)]. Here, the function \tanh is consistent with the mean-field form of the magnetization $\mu_i^\pm = \tanh(\beta \sum_{j \neq i} J_{ij} \mu_j^\pm)$. Meanwhile, in the RS2 phase, the regulated μ^+ and nonregulated μ^- states exhibit correlations with ξ_1 and ξ_2 , respectively, as shown in Fig. 4(b). In both phases, the correlations between μ^\pm and ξ_r ($r \geq 3$) are negligible.

In Figs. 5(a) and 5(b), we show the temperature dependence of the correlation between the eigenvectors and μ^\pm by introducing the correlation coefficient between $\{\xi_{ri}\}$ and $\{\text{atanh}(\mu_i^\pm)\}$ for $r = 1, 2, 3$. Here, the function atanh is in-

troduced by considering the tanh-form dependencies of μ^\pm on ξ_1 or ξ_2 , as shown in Fig. 4. We denote the vector consisting of $\text{atanh}(\mu_i^\pm)$ ($i = 1, \dots, N$) as $\text{atanh}(\mu^\pm) \in \mathbb{R}^N$. As shown in Fig. 5(a), the correlation coefficient between the first eigenvector ξ_1 and the mean phenotype with regulation μ^+ increases at $T < T_0$, namely, in the RS1 phase. As the temperature is lowered further below T_1 (toward the RS2 phase), the correlation between the regulated state and the second eigenvector increases to become larger than that between the first eigenvector and the regulated state. The asymmetry in this assignment, namely, the absence of genotypes with the relationship $\xi_1 \sim \mu^+$ or $\xi_2 \sim \mu^-$ in RS2 phase, originates from the definition of fitness Eq. (7). The number of configurations $\mathbf{S}_R (\notin \mathbf{S}_R^+)$ is larger than those of \mathbf{S}_R^+ . Hence, the expression of μ^- is preferred, and accordingly, the first eigenvector is assigned to the expression of μ^- .

Meanwhile, as shown in Fig. 5(b), the correlation between the first eigenvector and the nonregulated state μ^- is always higher than that of other eigenvectors at $T < T_0$. The correlations between the eigenvectors higher than the second order and the regulated or nonregulated states are small, as with ξ_3 shown in Figs. 5(a) and 5(b).

In summary, typical phenotypes evolved in the RS1 phase are concentrated on the direction of the first eigenvector, for both with and without regulation. Meanwhile, in the RS2 phase, the typical phenotypes with and without regulation are distinctively concentrated along the second and first eigenvectors of genotype, respectively. Thus, the typical phenotypes generated by two distributions $p_\beta^\pm(\mathbf{S}|\mathbf{J})$ are almost orthogonal to each other.

The contributions of the first and second eigenmodes to the mean phenotypes μ^\pm are given by the magnitudes of their corresponding eigenvalues. In Fig. 5(c), we show the T dependence of the expected value of the first, second, and third eigenvalues of the evolved genotypes. The horizontal lines denote their expected values for the symmetric matrices whose components independently and identically obey the uniform distribution over Ω_J . For $T < T_0$, the first eigenvalue shows a distinct increase from the expected value, whereas for $T \simeq T_1$, the second eigenvalue increases. Meanwhile, the third- and

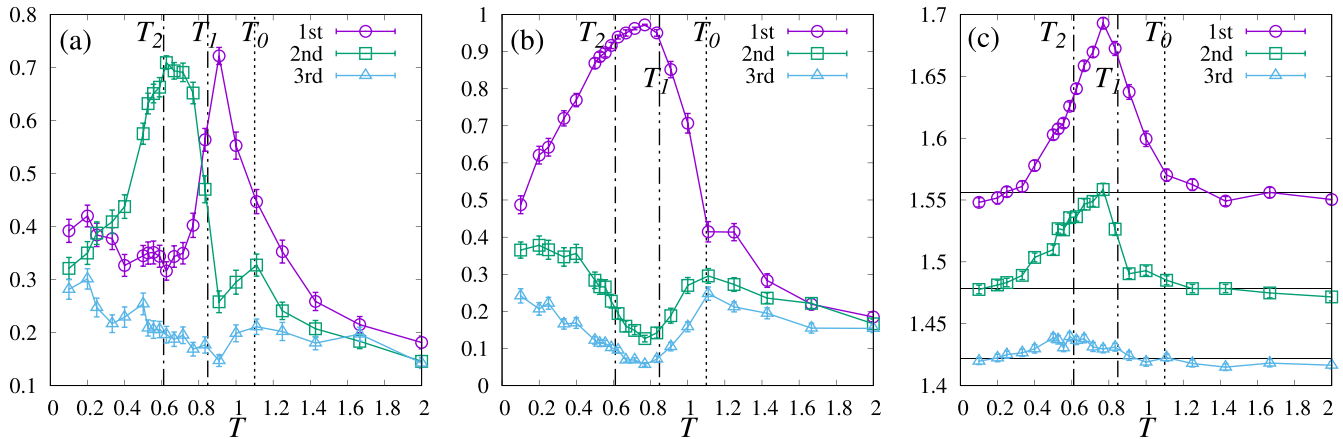


FIG. 5. The correlation coefficient between the first, second, and third eigenvectors with (a) regulated state μ^+ and (b) nonregulated state μ^- . The T dependence of the first, second, and third eigenvalues of the evolved genotypes is shown in (c), where the three horizontal lines represent the expected eigenvalues for randomly generated \mathbf{J} . The vertical dashed line, one-dot-chain line, and two-dot-chain line denote T_0 , T_2 , and T_1 , respectively. Each point is averaged over 100 samples of the evolved \mathbf{J} .

higher-order eigenvalues show slight changes. Therefore, the two desirable phenotypes are achieved by the contribution of the first- and second-order eigenmodes.

Following these observations, we map the mean phenotypes with and without regulation onto the two-dimensional space spanned by the first and second eigenvectors, ξ_1 and ξ_2 , of the evolved genotypes. In the RS1 and RS2 phases, characteristic mappings are observed, as shown in Fig. 6(a), where the mean phenotypes with and without regulation are denoted by \star and \bullet , respectively. In the RS1 phase, the first eigenvector is dominant to express both mean phenotypes with and without regulation for most of the evolved genotypes. We term this case as the overlapped phenotypes [Fig. 6(a) left]. Meanwhile, in the RS2 phase, phenotypes are shaped by the first and second eigenvectors of the evolved genotypes. These genotypes can satisfy the required fitness conditions both without and with regulation, respectively. Thus, we term

the case as separated phenotypes, as shown in Fig. 6(a) right. Hereafter, we term the genotype \mathbf{J} that gives overlapped and separable phenotypes as types J1 and J2, respectively.

Figure 6(b) shows the temperature dependence of the fraction of the type J1 and J2 genotypes among the ensemble of evolved genotypes $\mathcal{J}(T)$. At sufficiently large T , their fractions are equal to 0.25, which is indicated by horizontal lines. The value of 0.25 is the expected value of the fraction of types J1 and J2 for the randomly generated \mathbf{J} 's, as there are two other cases of mapping: the case that \star and \bullet located along ξ_2 and that \star and \bullet are along ξ_1 and ξ_2 , respectively. As T decreases toward the RS1 phase, the fraction of genotypes of type J1 increases to 0.8. By lowering the temperature further in the RS2 phase, the dominant genotype is replaced by type J2. For lower $T < T_1$, the dominance of type J2 decreases as T decreases, and the fraction of types J1 and J2 approaches 0.25.

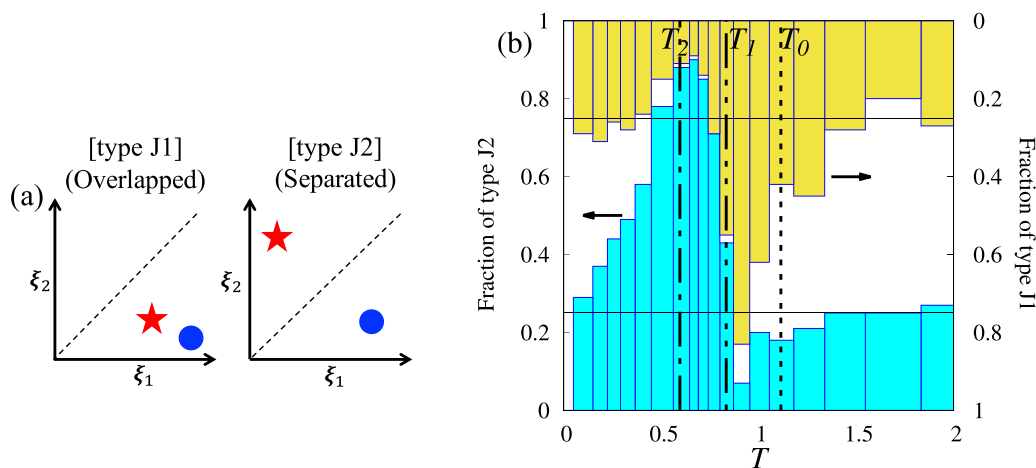


FIG. 6. (a) Characteristic mapping of the mean phenotypes with regulation (\star) and without regulation (\bullet), where the diagonal dashed line with a 45° slope is a guide for the eyes. (b) Fraction of genotypes of types J2 (cyan, left axis) and J1 (yellow, right axis). The horizontal lines represent 0.25, which is the trivial value for randomly distributed genotypes. The vertical dashed line, one-dot chain, and two-dot chain line represent T_0 , T_2 , and T_1 , respectively.

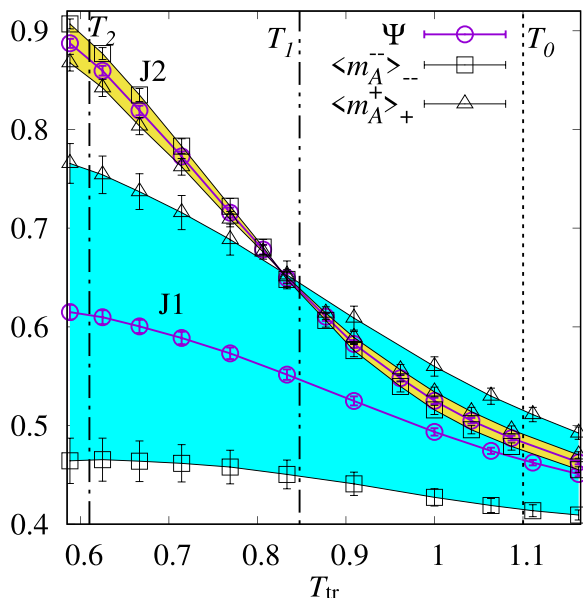


FIG. 7. Trial temperature T_{tr} dependence of the fitness for $\mathbf{J} \in \mathcal{J}(T)$ at $T = 0.91$ (denoted by J1) and $T = 0.63$ (denoted by J2). The shaded region indicates the difference between $\langle m_A^- \rangle_-$ and $\langle m_A^+ \rangle_+$.

C. Why do the type J2 genotypes appear at $T < T_1$?

Here, we discuss why type J1 and J2 genotypes are dominant at $T_1 < T < T_0$ and $T_2 < T < T_1$, respectively. To answer this question, we observe the fitness of the evolved genotypes $\mathcal{J}(T)$ under a trial temperature T_{tr} . The evolutionary process in our model selected genotypes among possible \mathbf{J} 's; hence, $\mathbf{J} \in \mathcal{J}(T)$ can be a candidate for genotypes in $\mathcal{J}(T_{tr})$ ($T \neq T_{tr}$), in principle. By evaluating the fitness of $\mathbf{J} \in \mathcal{J}(T)$ at a different temperature T_{tr} , we discuss the reason why $\mathbf{J} \in \mathcal{J}(T)$ cannot be selected at the trial temperatures.

Figure 7 shows the T_{tr} dependence of the fitness Ψ on $\mathbf{J} \in \mathcal{J}(T)$ for $T = 0.91$ (type J1; RS1) and $T = 0.63$ (type J2; RS2). At sufficiently large T_{tr} , fitness values of J1 and J2 do not differ much. Types J1 and J2 are subject to one- and two-dimensional constraints, respectively. More precisely, the first eigenvector of the type J1 genotypes needs to be in the direction that can express both phenotypes with and without regulation, and $N - 1$ eigenvectors can be freely determined [Fig. 6(a)]. Meanwhile, the first and second eigenvectors of the type J2 genotypes need to be in the direction of the two endpoint phenotypes to express distinct phenotypes depending on the regulation; the remaining $N - 2$ eigenvectors can be freely determined [Fig. 6(a)]. Hence, the possible configurations for type J1 are larger than those of type J2. From a thermodynamic perspective, the dominance of type J1 in the RS1 phase is caused by this entropic effect. In the RS2 phase, the fitness of type J2 is sufficiently large to overcome the entropic effect and hence can be dominant in this phase. This observation indicates that the changes in the ensemble of $\mathcal{J}(T)$ can be regarded as a phase transition with respect to genotypes between types J1 and J2.

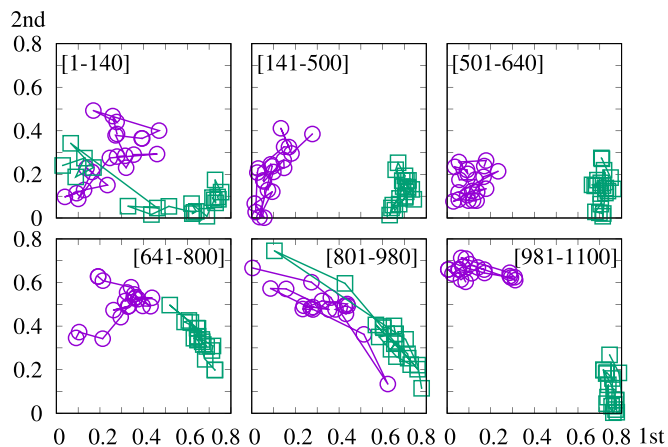


FIG. 8. The evolution of mean phenotypes. Corresponding to the evolution shown in Fig. 2(b), this figure shows the evolution of the mean phenotype in the two-dimensional space spanned by the first and second eigenvectors of the genotype for the evolution generations [1–140], [141–500], [501–640], \dots , [981–1100]. The results with and without regulations are plotted as \circ and \square , respectively.

D. Evolutional dynamics of genotypes on the two-dimensional plane

For understanding the evolutionary construction of the separated phenotypes, we simplify the evolutionary dynamics using the two-dimensional space spanned by the first and second eigenvectors, although the two-dimensional approximation was not necessarily accurate in the early stages of evolution, even in the RS2 phase. In Fig. 8, we show evolutionary change of the mean phenotypes in RS2 phase corresponding to the series shown in Fig. 2(b), where $\langle m_A^- \rangle_-$ increased before $\langle m_A^+ \rangle_+$. The panels of Fig. 8 show the time evolution of the mean phenotypes $\mu^+[\mathbf{J}^{(g)}]$ (\circ) and $\mu^-[\mathbf{J}^{(g)}]$ (\square) mapped onto the two-dimensional space spanned by the first and second eigenvectors of the genotype at each generation denoted in the panels. The localization of the mean phenotype without regulation appears on the first eigenvector 141–500 generations before that of the regulation case. From generations 641 to 800, the contribution of the second eigenvector to the mean phenotype increases with regulation. After the reorganization of the distributions at generations 801–980, the characteristic phenotype mapping for the type J2 genotype appears.

When $\langle |m_A^+| \rangle_+$ increases before the increase of $\langle |m_A^+| \rangle_-$, the localization of μ^+ on the second eigenvector appears during the early stage of evolution. Additionally, the localization of μ^- follows the reorganization of μ^+ . When both $\langle |m_A^\pm| \rangle_\pm$ increase simultaneously, μ^\pm localize almost simultaneously (see Appendix A).

IV. SWITCHING TRAJECTORY

Under the \mathbf{J} 's of type J2, the shift between the regulated and nonregulated states involves a large conformational change. We employ the MCMC method according to Eq. (1) for simulating the transition dynamics from regulated to nonregulated cases, or vice versa, and computed the MC steps required for the shift between the two cases.

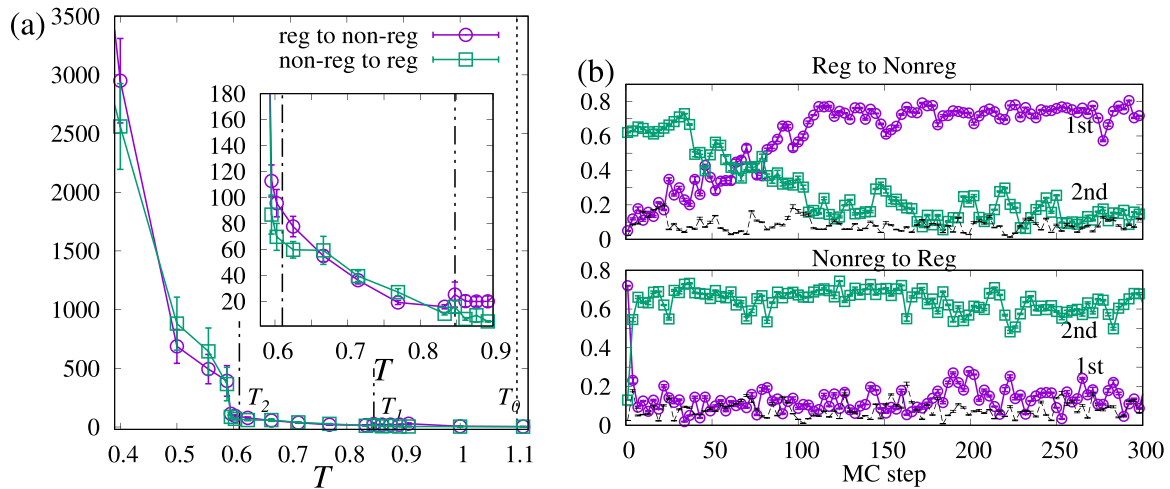


FIG. 9. (a) MC steps required for the switching from regulated to nonregulated state (\circ) and nonregulated to regulated state (\square). The dashed vertical, two-dotted chain, and one-dotted chain lines denote T_0 , T_1 , and T_2 , respectively. The inset magnifies the difference between the RS1 and RS2 phase. The transition time to shift the active sites from the nonregulated state to the regulated state was evaluated as follows. After sufficient time updates of \mathbf{S} under the nonregulated condition $\mathbf{S}_{\mathcal{R}} \notin \mathbf{S}_{\mathcal{R}}^+$, the regulatory sites were changed to $\mathbf{S}_{\mathcal{R}} \in \mathbf{S}_{\mathcal{R}}^+$, and then \mathbf{S} (except the regulatory region) was updated according to Eq. (1). We computed the target magnetization $|\sum_{i \in \mathcal{A}} S_i/N_{\mathcal{A}}|$ at each MC step to obtain the step where $|\sum_{i \in \mathcal{A}} S_i/N_{\mathcal{A}}|$ first reached the value $\langle |m_{\mathcal{A}}^+| \rangle_+$, which was defined as the transition time. (b) Switching trajectories of local magnetizations projected to the first and second eigenvectors defined on an evolved genotype at $T = 0.67$ (RS2). The component projected onto the third-order eigenvector is denoted by dashed lines.

Figure 9(a) shows the transition time calculated by the MCMC method from the regulated to nonregulated states (\circ) and from the nonregulated to regulated states (\square). Here, the upper limit of the MC step is set at 10^5 . In the RS1 phase, there is a minor change in phenotypes with and without regulation, and the transition time is within 20 steps. Compared with the RS1 phase, the transition time required in the RS2 phase is higher. This increase in relaxation time is associated with the large conformational change in the phenotype under the J2 genotypes. However, the large conformational change does not qualitatively change the relaxation time. As in the RS1 phase, the relaxation time in the RS2 phase is of the order of 10^2 . In the RSB phase, the MC steps required for switching diverge as T decreases. This phenomenon in the RSB phase is consistent with the property of the RSB phase where the metastable states hamper relaxation.

The trajectories shifting between two states lie in the 2^N -dimensional space. However, particularly in the RS2 phase, the two-dimensional space spanned by the first and second eigenvectors of the evolved genotype is sufficient to describe the switching trajectories. This low-dimensional constraint was already observed as the equilibrium property in the RS2 phase, as shown in Figs. 5(a) and 5(b). Figure 9(b) shows the trajectories of the components projected onto the first (\circ), second (\square), and third (dashed line) eigenvectors defined on an evolved \mathbf{J} of type J2 at $T = 0.67$ (RS2). During the regulated-to-nonregulated switching, the change in the first component is much larger, and in case of nonregulated-to-regulated switching, the change in the second component is much larger. Meanwhile, the third-order (and higher) components are nearly constant during regulated-to-nonregulated or nonregulated-to-regulated switching.

We generated 1000 switching trajectories on a certain $\mathbf{J} \in \mathcal{J}(T)$ and mapped them onto the two-dimensional space

spanned by the first and second eigenvectors of the evolved genotypes. Figure 10 shows the heat map on the two-dimensional space for the switching trajectories defined on an evolved genotype of type J2 at $T = 0.68$ (RS2) from nonregulated to regulated states. The mean phenotypes with and without regulation, μ^+ and μ^- , after sufficient time steps of updating are denoted by \star and \bullet , respectively. Additionally, the direction of fluctuation of these points is indicated by two lines below the points. The switching trajectory when regulation is removed is shown in Appendix B. For both cases of switching, most of the trajectories follow a quarter-circle path. This quarter-circle path is restricted to a one-dimensional path within the two-dimensional space. With this restriction, the transition time between the two states remains small, even though the two phenotypes are far apart, as shown in Fig. 9(a).

The quarter-circle path on the two-dimensional plane restricts the trajectories of the convergence from arbitrary initial conditions to the phenotypes with and without regulation. The heat map for the relaxation dynamics on a type J2 genotype evolved at $T = 0.67$ from arbitrary initial conditions is shown in Fig. 11 for the regulated case. Most of the trajectories are attracted once to the quarter-circle line where the switching paths are concentrated and then approach the regulated state. (The relaxation dynamics of the nonregulated phenotype are shown in Appendix B.) The quarter-circle path is attractive because any state moves forward to the regulated or nonregulated state through this path.

V. TWO-DIMENSIONAL APPROXIMATION OF FREE ENERGY LANDSCAPE

To understand the characteristic switching path in the two-dimensional space, we examined the free energy landscape.

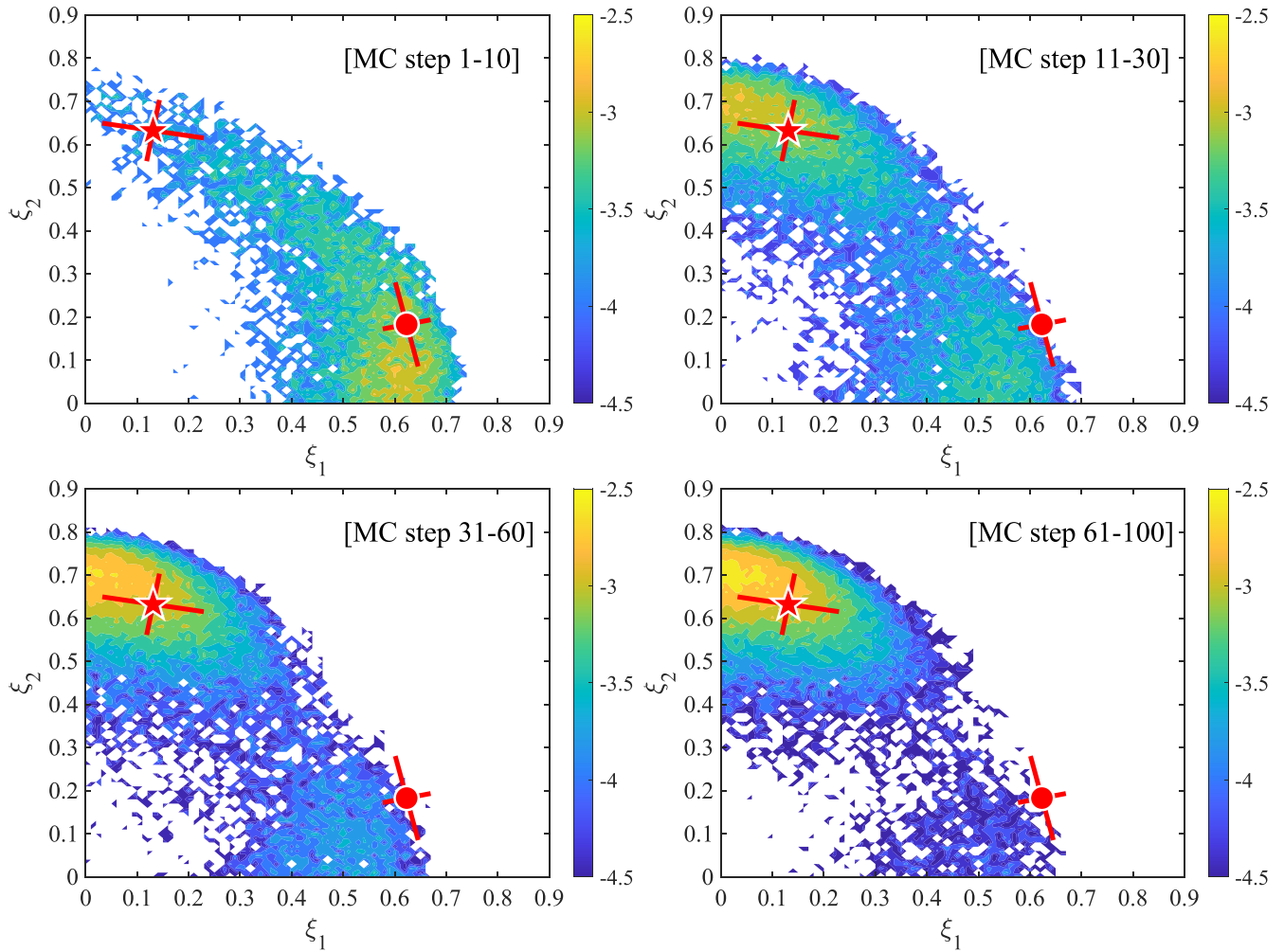


FIG. 10. Heat maps of the two-dimensional space for switching trajectories from regulated to nonregulated state, defined on an evolved genotype at $T = 0.67$ (RS2). Here, the two-dimensional space is meshed by 0.01, and \log_{10} frequencies of the trajectories during the given steps are plotted. \star and \bullet denote the regulated state and nonregulated state projected onto the two-dimensional space, respectively. The lines below these points represent the first and second eigenmodes of fluctuation around these points. Here, the length of the lines is magnified to be discernible. However, the ratio of the lines is proportional to the root of the ratio of the eigenvalues.

The free energies for the regulated and nonregulated cases, denoted by f_+ and f_- , are defined as

$$f_+ = -\frac{1}{N\beta} \ln \sum_{\mathbf{S} | \mathbf{S}_{\mathcal{R}} \in \mathcal{S}_{\mathcal{R}}^+} \exp(-\beta H), \quad (11)$$

$$f_- = -\frac{1}{N\beta} \ln \sum_{\mathbf{S} | \mathbf{S}_{\mathcal{R}} \notin \mathcal{S}_{\mathcal{R}}^+} \exp(-\beta H). \quad (12)$$

Following the result of the numerical simulations, we considered the two-rank approximation of the evolved \mathbf{J} as $\mathbf{J} \simeq \lambda_1 \xi^1 \xi^{1\top} + \lambda_2 \xi^2 \xi^{2\top}$. Under the two-rank approximation, the Hamiltonian is given by

$$H = -\sum_{k=1}^2 \frac{\lambda_k}{2} \left\{ \left(\sum_{i=1}^N \xi_i^k S_i \right)^2 - 1 \right\}. \quad (13)$$

The last term is put in to discard the contribution from the diagonal components. For the two-rank approximation form, one can represent the free energy as a function of m_1 and m_2 defined by

$$m_1^\pm = \frac{1}{\sqrt{N}} \xi^{1\top} \mu^\pm, \quad (14)$$

$$m_2^\pm = \frac{1}{\sqrt{N}} \xi^{2\top} \mu^\pm, \quad (15)$$

where m_1^+ and m_2^+ correspond to the projection of the local magnetization with regulation onto the first and second eigenvectors, respectively, whereas m_i^- ($i = 1, 2$) are those without regulation. By following the standard calculation in the literature [46,47], as is shown in Appendix C, the free

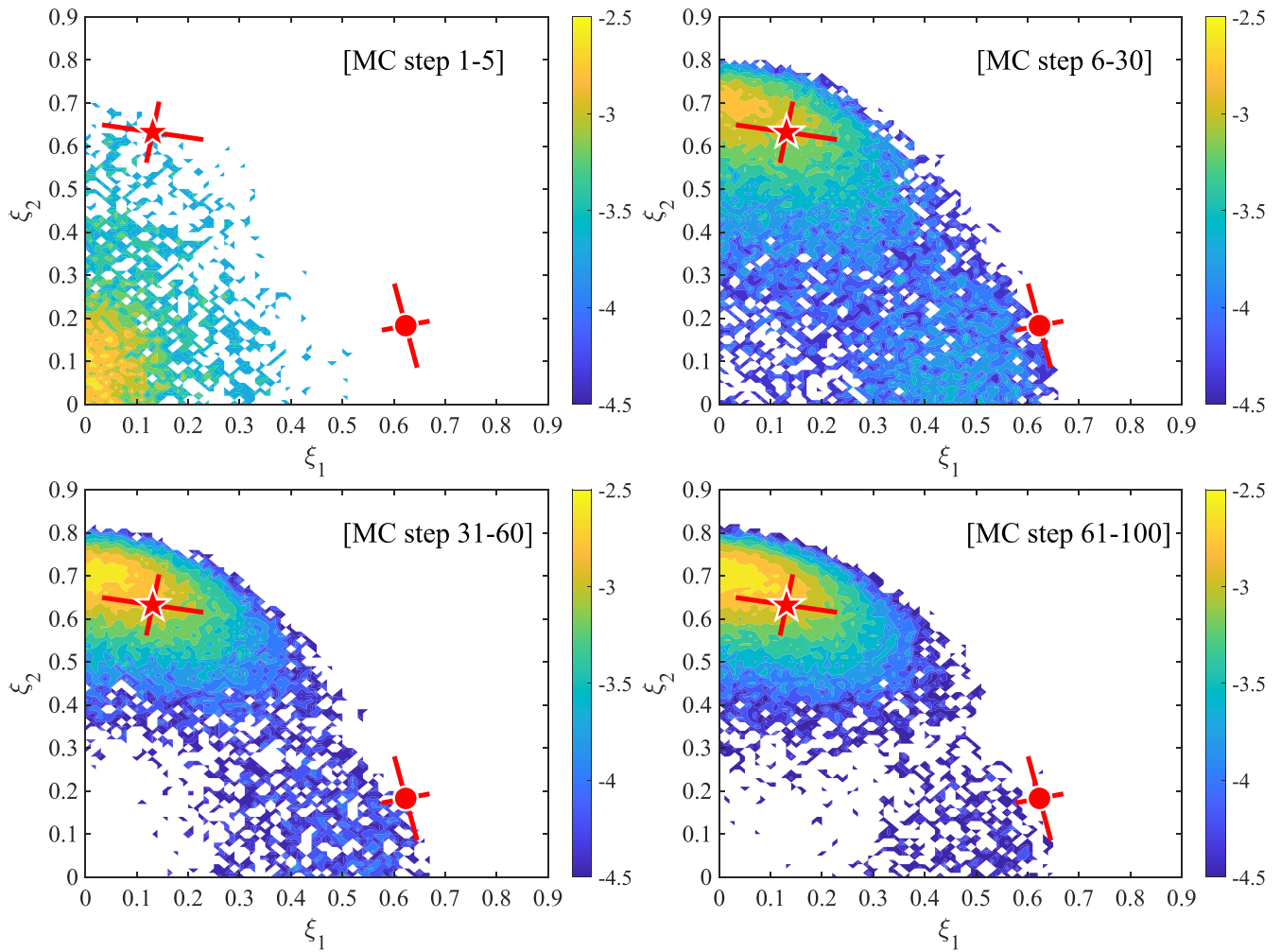


FIG. 11. Heat maps of the two-dimensional space for relaxation trajectories from an initial condition to the regulated state defined on the evolved genotype of type J2 at $T = 0.67$ (RS2), the same value as adapted in Fig. 10. \star , \bullet , and the orthogonal lines below these points are the same as in Fig. 10.

energies are given by

$$f_+ = \sum_{k=1}^2 \frac{\lambda_k m_k^{+2}}{2} - \frac{1}{N\beta} \left\{ \sum_{i=1}^N \ln[2 \cosh(\beta h_i^+)] + \ln(p_+^+ + p_-^+) \right\} + \frac{1}{N} \sum_{i < j, i, j \in \mathcal{R}} J_{ij}, \tag{16}$$

$$f_- = \sum_{k=1}^2 \frac{\lambda_k m_k^{-2}}{2} - \frac{1}{N\beta} \left\{ \sum_{i=1}^N \ln[2 \cosh(\beta h_i^-)] + \ln[1 - (p_+^- + p_-^-)] \right\}, \tag{17}$$

where $h_i^\pm = \lambda_1 m_1^\pm \sqrt{N} \xi_i^1 + \lambda_2 m_2^\pm \sqrt{N} \xi_i^2$ and

$$p_\pm^\pm = \prod_{i \in \mathcal{R}} \frac{\exp(\pm \beta h_i^\pm)}{2 \cosh(\beta h_i^\pm)}, \quad p_\pm^\mp = \prod_{i \in \mathcal{R}} \frac{\exp(\pm \beta h_i^\mp)}{2 \cosh(\beta h_i^\mp)}. \tag{18}$$

The saddle point equations for m_k^\pm are given by

$$m_k^+ = \frac{1}{\sqrt{N}} \sum_{i \notin \mathcal{R}} \xi_i^k \tanh(\beta h_i^+) + \frac{1}{N} \sum_{j \in \mathcal{R}} \xi_j^k \frac{p_+^+ - p_-^+}{p_+^+ + p_-^+}, \tag{19}$$

$$m_k^- = \frac{1}{\sqrt{N}} \sum_{i \notin \mathcal{R}} \xi_i^k \tanh(\beta h_i^-) + \frac{1}{\sqrt{N}} \sum_{i \in \mathcal{R}} \xi_i^k \frac{\tanh(\beta h_i^-) - (p_+^- - p_-^-)}{1 - (p_+^- + p_-^-)}. \tag{20}$$

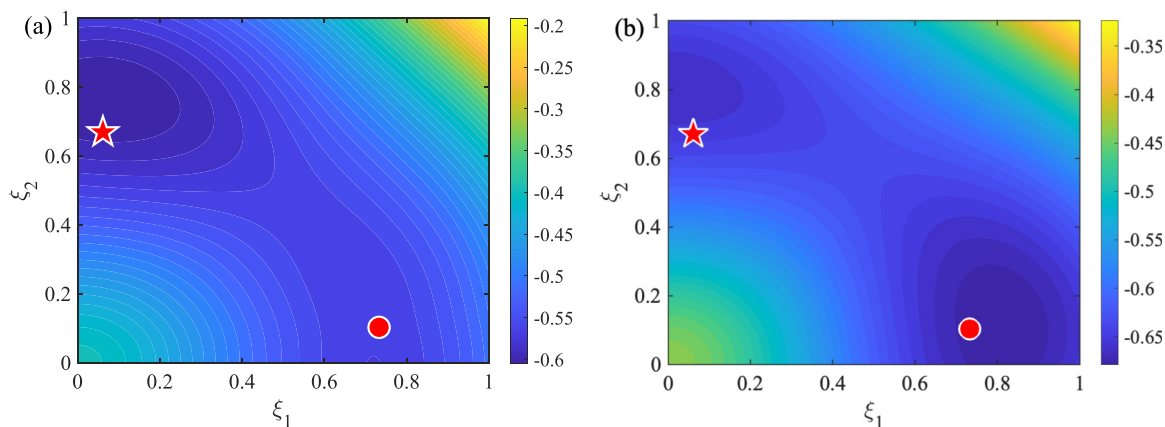


FIG. 12. Two-dimensional approximation of the free energy landscape of one genotype with separable phenotype space for (a) regulated state and (b) nonregulated state at $p_A = 0.05$ and $p_R = 0.1$. \star and \bullet show the projection of the regulated and nonregulated states, respectively.

Figures 12(a) and 12(b) show the landscape of f^+ and f^- , respectively, plotted on the two-dimensional space of one evolved J2 genotype in the RS2 phase at $T = 0.67$. The minima of the free energies are consistent with the numerically observed phenotypes with and without regulation, which are indicated by \star and \bullet ; hence, the two-dimensional approximation of the free energy is valid. As shown in Fig. 12, along the quarter-circle shape that connects the regulated and nonregulated states, the free energy remains small. The trajectories shown in Fig. 10 are restricted to this quarter-circle, wherein free energy is small.

Rough approximation of free energy

Further, we investigated what property of the evolved genotype gives the quarter-circle shape of the free energy landscape. We introduced the following assumptions:

- A1 : The difference between the first and second eigenvalues is negligible.
- A2 : The components of the eigenvectors ξ^1 and ξ^2 are independently and identically distributed, according to the Gaussian distribution $\mathcal{N}(0, 1/N)$.
- A3 : The active and regulatory sites are negligible.

Following the assumption **A1**, we replaced the first and second eigenvalues λ_1 and λ_2 with their mean $\bar{\lambda}$. Under these assumptions, we obtained the following form of free energy, as explained in the Appendix C:

$$f_{\text{app}} = \frac{\bar{\lambda}}{2} (m_1^2 + m_2^2) - \frac{1}{\beta} \int Dz \ln \cosh (\beta \bar{\lambda} \sqrt{m_1^2 + m_2^2} z), \quad (21)$$

where $Dz = \frac{dz}{\sqrt{2\pi}} \exp(-\frac{z^2}{2})$. The form of Eq. (21) indicates that the free energy under the approximations **A1–A3** depends on m_1 and m_2 through $m_S \equiv \sqrt{m_1^2 + m_2^2}$. Hence, the approximated free energy has the same value as per m_S , even when the individual values of m_1 and m_2 are different. The saddle

point of m_S is given by

$$m_S = \int Dz z \tanh(\beta \bar{\lambda} m_S z). \quad (22)$$

Figure 13 shows the free energy landscape under the assumptions **A1–A3** defined on a J2 genotype evolved at $T = 0.67$ (RS2). As expected from the form of Eq. (21), the approximated free energy shows a quarter-circle landscape. The quarter-circle curve represents the minimum free energy f_{app} , whereas the equilibrium states with and without regulation are denoted by stars and circles, respectively, which are located near the extremum line of f_{app} . Therefore, the one-dimensional and quarter-circle switching path is considered to be provided by the free sites, as the active and regulatory sites are ignored in deriving f_{app} (assumption **A3**). A particular difference between f_{\pm} and f_{app} is that the valleys around the mean of the phenotype with and without regulation (Fig. 12) cannot be described by f_{app} . For the description of these valleys, it is necessary to consider the active and regulatory sites. Thus, free energy consists of quarter-circle switching paths provided by free sites and valleys around the mean

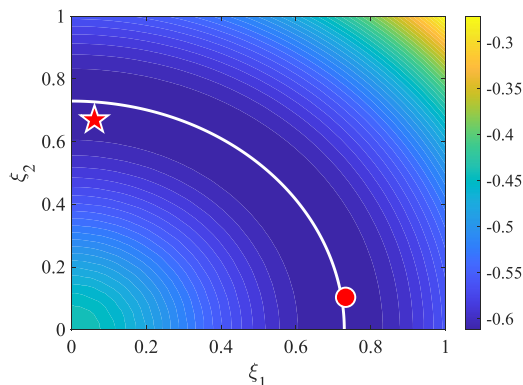


FIG. 13. Free energy landscape on the two-dimensional plane under the assumptions **A1–A3** at $T = 0.67$ (RS2). The solid line represents the minimum free energy, and the star and circle represent the mean of phenotypes with and without regulation, respectively.

phenotypes which in turn are provided by active and regulatory sites. Further, the assumption **A2** suggests that randomness in the embedded pattern in the free sites is significant for the description of the quarter-circle path. Therefore, as the number of free sites decreases, or equivalently, as the number of active and regulatory sites increases, the description by f_{app} would be invalid.

The importance of the interaction within the free sites is consistent with the Hopfield model [37]. The interference between two phenotypes that hampers stable expression is mitigated by the free sites, whose phenotypes with and without regulation are almost orthogonal, and the robust expression of two phenotypes is achieved.

VI. SUMMARY AND CONCLUSIONS

In this paper, we investigated the evolution of a spin model to generate two specific configurations of active sites depending on the regulation. A fitness function was designed to increase when the appropriate spin configurations (phenotypes) with and without regulation appeared with high probability. Our analysis revealed three transition points T_0 , T_1 , and T_2 . The fitness increased from the trivial value for $T < T_0$. For $T_2 < T < T_0$, the evolved system belonged to the RS phase. The RS phase was further divided into two regions at $T = T_1$, RS1 ($T_1 < T < T_0$) and RS2 ($T_2 < T < T_1$) phases, with dominant genotypes differing in type J1 and J2 regions for RS1 and RS2 phases, respectively. For $T_1 < T < T_0$, the phenotypes, i.e., spin configurations, other than active sites barely depended on the regulation. In contrast, for $T_2 < T < T_1$, the two phenotypes with and without regulation, showed a large difference, contrasting the small difference in the RS1 phase.

In the RS2 phase, the two phenotypes were provided by using the first and second eigenmodes to express nonregulated and regulated phenotypes, respectively, where the switching path between the two phenotypes can be described by the first and second eigenmodes of the two endpoint phenotypes. A one-dimensional quarter-half shape switching path connected the two endpoint phenotypes in the two-dimensional space spanned by the first and second eigenvectors of the J2 genotype. This switching path was robust to perturbations, in the sense that any trajectories deviating from the path were attracted to the path. Evolutionary construction of this one-dimensional path met the requirements of plasticity against regulatory changes and robustness in phenotypes. Further, the low-dimensionality of the switching path allowed for quick switching between two stable phenotypes depending on the regulation.

To understand the evolutionary origin of the one-dimensional switching path, we applied a two-dimensional approximation to the free energy landscape for the evolved genotype in the RS2 phase. By only considering randomness in the free sites of two endpoint phenotypes, it was found that the free energy takes a minimum along a quarter-circle shape in two dimensions. The two endpoint phenotypes were located near the quarter-circle path, and the switching trajectories followed the valley of the free energies connecting the two endpoints. In this case, the minima relate to the sites that were active and regulated. The cooperative evolution of the active,

regulatory, and free sites provided stable expression of the endpoint phenotypes and robust switching paths.

Our findings suggest that low dimensionality plays a crucial role in achieving both stable expressions of two phenotypes and large conformational changes over a stable path. This leads to the acquisition of both robustness and plasticity. Constraints on adaptive changes in phenotypes upon environmental and evolutionary changes have recently received much attention [29,31,48,49]. The constraint attracts a low-dimensional subspace within the high-dimensional space, supporting the robustness. Here, we demonstrated that the state change relevant to function is facilitated by the one-dimensionally constrained path on the two-dimensional plane, which allows large-amplitude plastic motion that is advantageous for functional changes. Notably, this constrained path is already prepared as a relaxation path during the course of evolution (Fig. 8).

Authors of previous studies have demonstrated that genotypes providing a single function by expressing a specific phenotype can evolve in the RS phase [31]. In this paper, we found a transition that occurs in the RS phase for two-functional phenotypes. The genotypes that achieve switching between two functional phenotypes depending on the regulation were dominant in the RS2 phase, i.e., in the temperature region closer to the RSB within the RS phase. For the evolution to achieve more functions, further transitions within the RS phase can be expected. With such successive transitions, the genotype will approach the RSB transition point, where further plasticity will be achieved. This may be consistent with the observation of critical behavior in protein dynamics [30], wherein plasticity and robustness are compatible.

Here, we did not impose any driving force to create the one-dimensional switching path. Rather, the evolution under fitness defined by the two endpoint phenotypes resulted in genotypes that provide not only stable expression of the phenotypes but also robust and plastic switching. This observation presents the possibility of evolutionary construction of proteins [50] with allosteric effects based on the binding ability of the active site, under conditions characterized by the RS phase, in addition to synthetic approaches [51]. Notably, in this paper, we demonstrated that a fitness function without imposing rapid and robust switching can provide switching characteristics as observed in real proteins, when the temperature is within an appropriate range and sufficient free sites exist. Further analysis of interacting spin systems that achieve robust multiple functions is essential for the evolution of proteins and material design [52,53].

Investigation of the microscopic properties of evolved genotypes is an important dimension of future research. However, the focus of this paper was on the extraction of macroscopic low-dimensional structures. Frustration is a potential measure to characterize the genotype, which captures consistency in interaction. An increase in frustration can indicate a rugged landscape. Generally, as the number of embedded patterns increases, the level of frustration in the interactions increases [37,54]. We observed an increase in frustration in our model in comparison with the one-desirable phenotype case (Appendix D). In actual proteins, steric frustration can be utilized by multisubstrate enzymes to facilitate

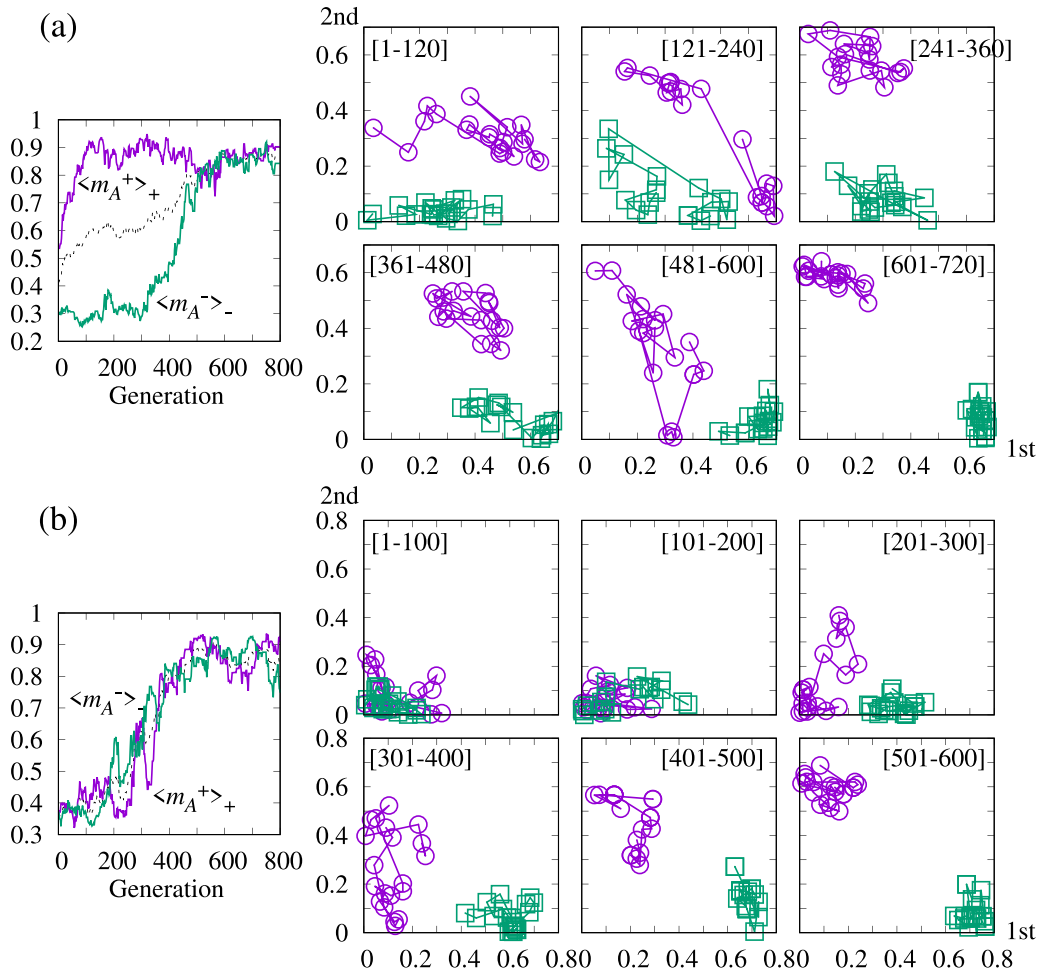


FIG. 14. Examples of evolutionary dynamics in two-dimensional space in the RS2 phase.

the rate-limiting product-release step [55]. Understanding the relationship between frustration and the number of embedded patterns may provide insights into the properties of real biomolecules.

The evolutionary spin model considered in this paper is rather simple and abstract. There is room for considering more realistic settings and discussing the generality of the results. For instance, several biological molecules have multiple regulatory or active sites, and their phenotype expression is more complicated. The G protein-coupled receptors show dual ligand binding events where the binding of one ligand enhances that of the other [56,57]. Thiamine diphosphate in the two active sites of pyruvate dehydrogenase complex can communicate with each other over a distance of 20 Å using a proton to switch the conformation [58]. The contribution of such cooperation to the evolution of robustness and plasticity needs to be revealed. In contrast with the global coupling model, the study of models with spatially localized interactions is also important [59–61]. From the insights based on the Markov network model, which encompasses our model as well, our conclusion regarding the significance of the free sites will be valid and independent of the details of the model setting [41]. However, there might be quantitative variations, which need further investigations.

In conclusion, we showed that the stable expression and switching of phenotypes takes advantage of evolutionary constructed low-dimensional phenotypic constraints, with which robustness and plasticity are compatible. Our findings here may be interesting in possible relationship with recent studies on evolutionary dimensional reduction [29,31,48,49].

ACKNOWLEDGMENTS

The authors thank Qian Yuan Tang and Tuan Pham for helpful comments and discussions. This paper is partially supported by Grant-in-Aid for Scientific Research (A) (No. 20H00123) from the Ministry of Education, Culture, Sports, Science, and Technology (MEXT) of Japan. K.K. is also supported by the Novo Nordisk Foundation (NNF21OC0065542).

APPENDIX A: EVOLUTIONAL DYNAMICS OF THE GENOTYPES ON THE TWO-DIMENSIONAL PLANE

Figure 14 shows evolutionary dynamics of $\langle m_A^\pm \rangle_\pm$ for the cases (a) $\langle m_A^+ \rangle_+$ increases before $\langle m_A^- \rangle_-$, and (b) $\langle m_A^\pm \rangle_\pm$ increases simultaneously, as indicated by the left panels. The right six panels show the evolution of local magnetization in

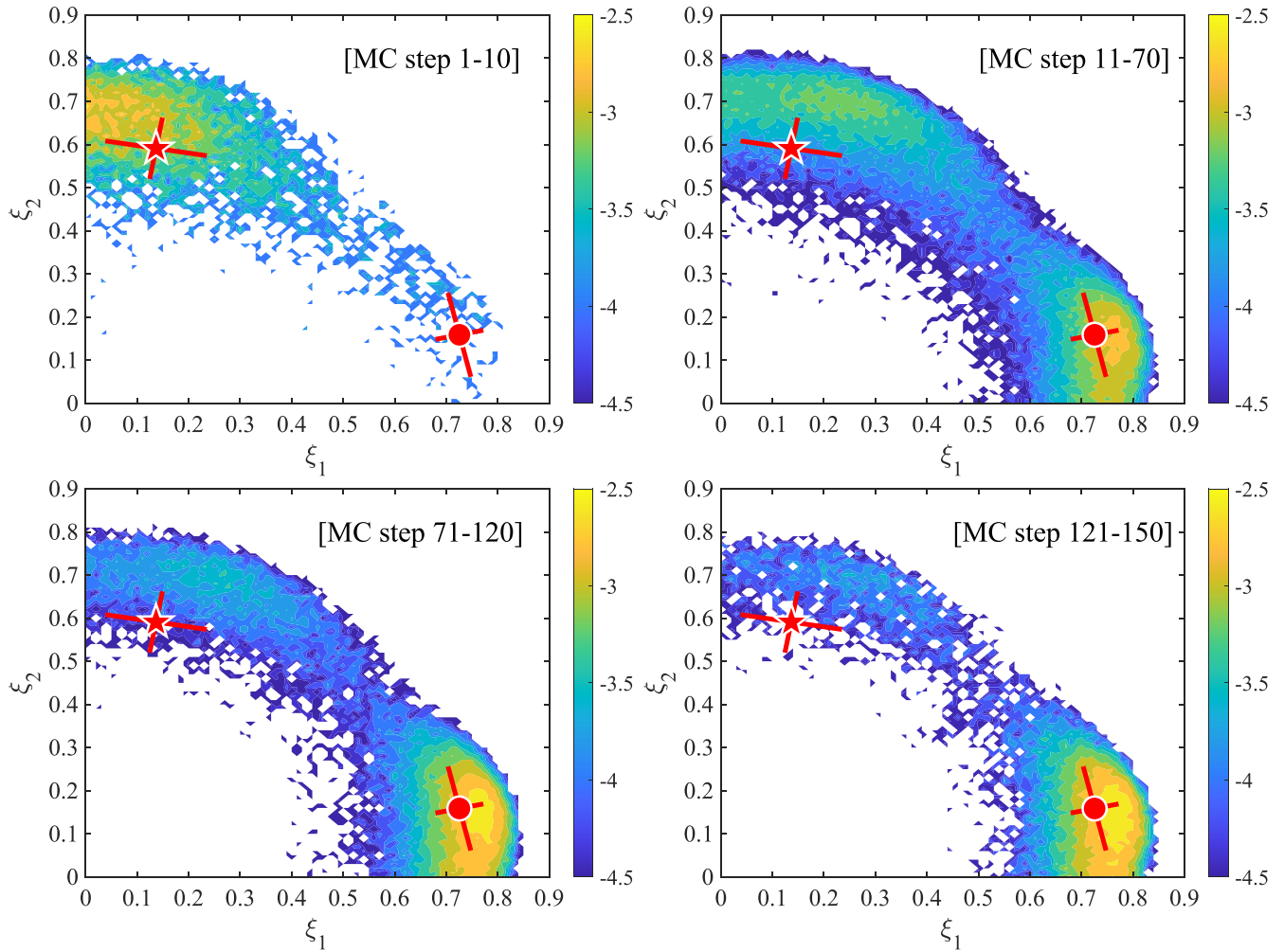


FIG. 15. The heat map illustrates two-dimensional switching trajectories from regulated to nonregulated state, defined on the evolved genotype type J2 at $T = 0.67$ (RS2), the same as that used in Fig. 10. Star, square, and orthogonal lines below these points are the same as in Fig. 10.

the two-dimensional space spanned by the first and second eigenvectors of the genotype at the evolutionary step. This is indicated at the right top of the panels. The circles and squares denote the regulated and the nonregulated states, respectively. The case where $\langle m_A^- \rangle_-$ increases before $\langle m_A^+ \rangle_+$ is shown in Fig. 8.

APPENDIX B: REGULATED TO NONREGULATED STATE

Figure 15 shows the switching trajectory from the case with regulation to without regulation in the evolved J2 genotype, as shown in Fig. 10. Figure 16 shows the convergence to the nonregulated state starting from arbitrary initial conditions.

APPENDIX C: DERIVATION OF THE FREE ENERGY DENSITY

We introduced the equality:

$$1 = \int dm_k \delta \left(m_k - \frac{1}{\sqrt{N}} \sum_{i=1}^N \xi_i^k S_i \right),$$

for $k = 1, 2$ to the partition function with regulation as

$$Z_+ = \int dm_1^+ dm_2^+ \sum_{S|S_{\mathcal{R}}^+ \in S_{\mathcal{R}}} \prod_{k=1}^2 \delta \left(m_k - \frac{1}{\sqrt{N}} \sum_{i=1}^N \xi_i^k S_i \right) \exp \left[\sum_{k=1}^2 \frac{\beta \lambda_k}{2} (m_k^2 - 1) \right]$$

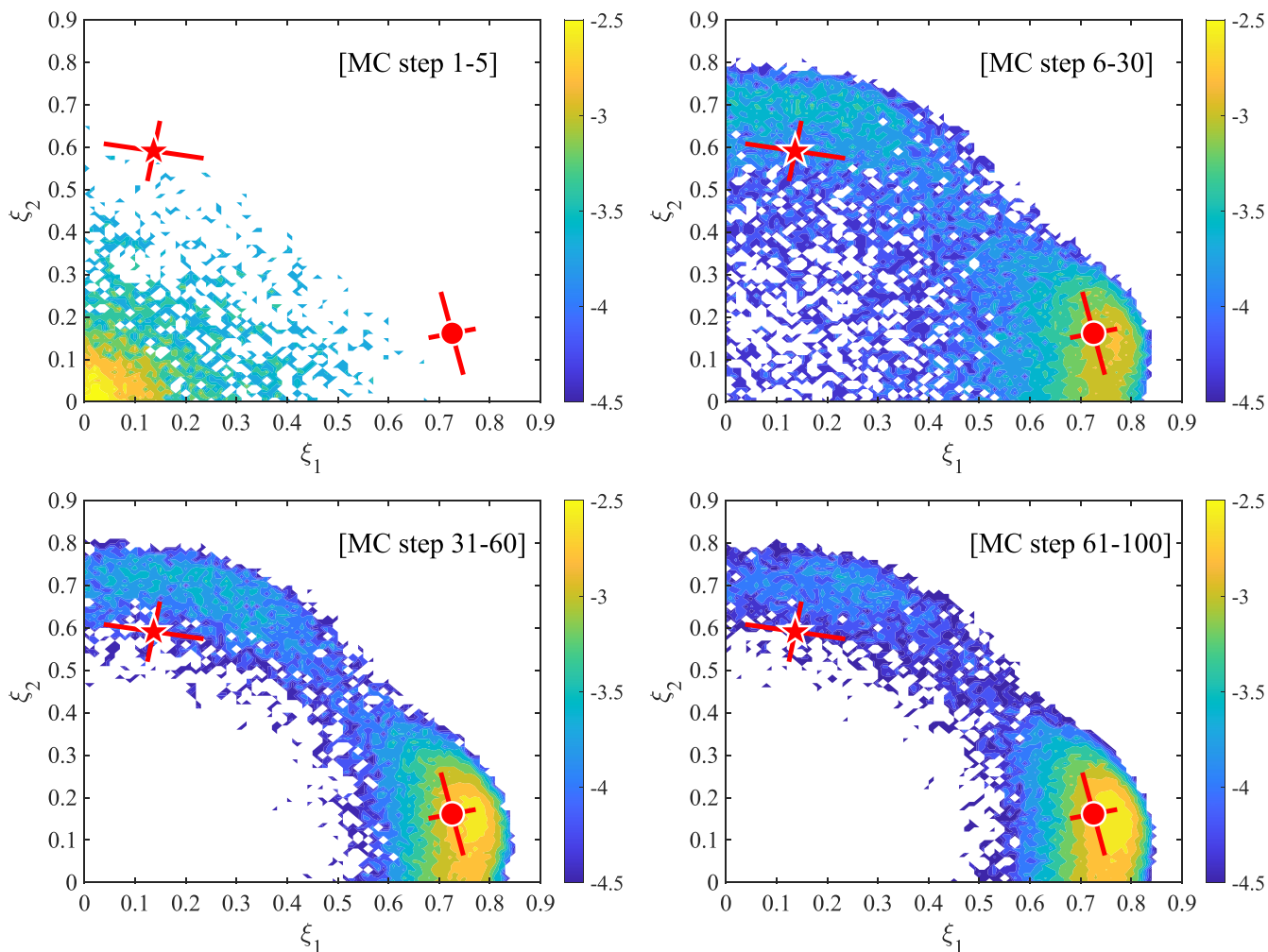


FIG. 16. Heat map on the two-dimensional space for relaxation trajectories from an initial condition to the nonregulated state defined in the evolved genotype of type J2, as shown in Fig. 11. Star, square, and the orthogonal lines below these points are the same as in Fig. 11.

$$\begin{aligned}
 &= \int dm_1^+ dm_2^+ d\hat{m}_1^+ d\hat{m}_2^+ \sum_{\mathbf{S}|\mathbf{S}_{\mathcal{R}}^+ \in \mathcal{S}_{\mathcal{R}}} \prod_{k=1}^2 \exp \left[-Nm_k \hat{m}_k + \sqrt{N} \hat{m}_k \sum_{i=1}^N \xi_i^k S_i + \frac{\beta \lambda_k}{2} (m_k^2 - 1) \right] \\
 &= \int dm_1^+ dm_2^+ d\hat{m}_1^+ d\hat{m}_2^+ \prod_{k=1}^2 \exp \left[-Nm_k \hat{m}_k + \frac{\beta \lambda_k}{2} (m_k^2 - 1) \right] \\
 &\quad \times \prod_{i=1}^N \left\{ 2 \cosh \left(\sqrt{N} \sum_{k=1}^2 \hat{m}_k \xi_i^k \right) \right\} \{p_+^+ + p_-^+\}. \tag{C1}
 \end{aligned}$$

The integrals were implemented by utilizing the saddle point method [46,47].

For the nonregulated case, we obtained

$$\begin{aligned}
 Z_- &= \int dm_1^- dm_2^- d\hat{m}_1^- d\hat{m}_2^- \sum_{\mathbf{S}|\mathbf{S}_{\mathcal{R}} \notin \mathcal{S}_{\mathcal{R}}^+} \prod_{k=1}^2 \exp \left[-Nm_k \hat{m}_k + \sqrt{N} \hat{m}_k \sum_{i=1}^N \xi_i^k S_i + \frac{\beta \lambda_k}{2} (m_k^2 - 1) \right] \\
 &= \int dm_1^- dm_2^- d\hat{m}_1^- d\hat{m}_2^- \prod_{k=1}^2 \exp \left[-Nm_k \hat{m}_k + \frac{\beta \lambda_k}{2} (m_k^2 - 1) \right] \\
 &\quad \times \prod_{i=1}^N \left\{ 2 \cosh \left(\sqrt{N} \sum_{k=1}^2 \hat{m}_k \xi_i^k \right) \right\} \times \{1 - (p_+^- + p_-^-)\}. \tag{C2}
 \end{aligned}$$

1. Free energy under assumptions A1–A3

Under the assumptions A1 and A3, $Z^+ = Z^-$ holds, and we denote it as Z_{\pm} given by

$$\begin{aligned}
 Z_{\pm} &= \sum_{\mathbf{S}} \exp \left[\beta \bar{\lambda} \sum_{i < j} (\xi_i^1 \xi_j^1 + \xi_i^2 \xi_j^2) S_i S_j \right] \\
 &\sim \sum_{\mathbf{S}} \int dm_1 dm_2 \delta \left(m_1 - \frac{1}{\sqrt{N}} \sum_{i=1}^N \xi_i^1 S_i \right) \\
 &\quad \delta \left(m_2 - \frac{1}{\sqrt{N}} \sum_{i=1}^N \xi_i^2 S_i \right) \exp \left[\frac{\beta \bar{\lambda} N}{2} (m_1^2 + m_2^2) \right] \\
 &= \int dm_1 dm_2 d\hat{m}_1 d\hat{m}_2 \exp(-N\hat{m}_1 m_1 - N\hat{m}_2 m_2) \\
 &\quad \exp \left[\frac{\beta \bar{\lambda} N}{2} (m_1^2 + m_2^2) \right] \\
 &\quad \times \prod_i 2 \cosh(\hat{m}_1 \sqrt{N} \xi_i^1 + \hat{m}_2 \sqrt{N} \xi_i^2) \\
 &= \int dm_1 dm_2 \exp \left\{ -\frac{\beta \bar{\lambda} N}{2} (m_1^2 + m_2^2) \right. \\
 &\quad \left. + \sum_i \ln \cosh \left[\beta \bar{\lambda} \sqrt{N} (m_1 \xi_i^1 + m_2 \xi_i^2) \right] \right\}, \quad (\text{C3})
 \end{aligned}$$

Here, we introduced the saddle point method for the integrals with respect to \hat{m}_1 and \hat{m}_2 . Under the assumption A2, when the system size is sufficiently large, the summation with respect to the components of the eigenvectors can be replaced with the integral according to the Gaussian distribution as

$$\begin{aligned}
 Z_{\pm} &= \int dm_1 dm_2 \exp \left[-\frac{\beta \bar{\lambda} N}{2} (m_1^2 + m_2^2) \right. \\
 &\quad \left. + N \int Dz \ln \cosh(\beta \bar{\lambda} \sqrt{m_1^2 + m_2^2} z) \right]. \quad (\text{C4})
 \end{aligned}$$

By introducing the saddle point method to the integrals of m_1 and m_2 , we obtained the approximated free energy f_{app} .

APPENDIX D: FRUSTRATION

We investigate how the configuration of genotypes changes through evolution depending on temperature. We focus on the triplets of interactions $J_{ij}J_{jk}J_{ki}$. From the form of Hamiltonian, the expression of phenotypes that satisfy $S_i S_j = \text{sign}(J_{ij})$, $S_j S_k = \text{sign}(J_{jk})$, and $S_k S_i = \text{sign}(J_{ki})$ is preferred to minimize the interaction energy $-(S_i J_{ij} S_j + S_j J_{jk} S_k + S_k J_{ik} S_i)$ when the triplets take a positive value. However, if the triplets take a negative value, namely, frustrated, there is no unique configuration of S_i , S_j , and S_k to minimize the

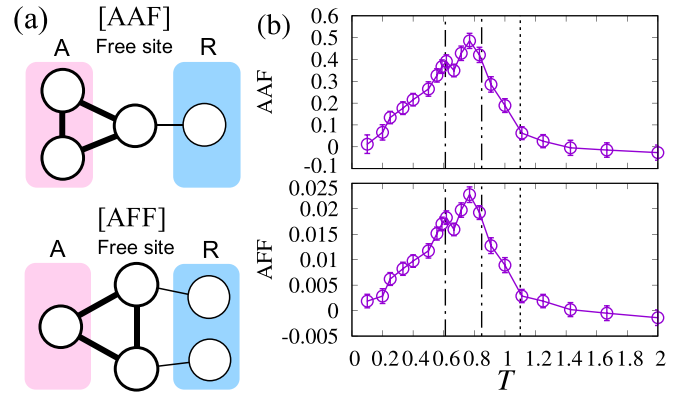


FIG. 17. (a) Schematic pictures of less frustrated plaquettes in the RS2 phase. (b) Temperature dependence of the mean of triplets Δ_{AAF} and Δ_{AFF} among 100 samples of evolved $\mathbf{J} \in \mathcal{J}(T)$ after 10^5 generations.

term $-(S_i J_{ij} S_j + S_j J_{jk} S_k + S_k J_{ik} S_i)$. Frustration is an obstacle to attaining the unique energy minimum. Authors of a previous study showed that frustration is suppressed by evolution to achieve robust phenotype expression with funnel type dynamics [32].

In our model, we set active, regulatory, and remaining free sites where the fitness is quantified through the active and regulatory sites. The direct connection between the active and regulatory sites is prohibited when we consider the allosteric interaction between them. Hence, we introduced the following mean of triplets:

$$\Delta_{\text{AAF}} = \frac{1}{\sum_{i,j \in \mathcal{A}} \sum_{k \in \mathcal{F}} |J_{ij} J_{jk} J_{ki}|} \sum_{i,j \in \mathcal{A}} \sum_{k \in \mathcal{F}} J_{ij} J_{jk} J_{ki}, \quad (\text{D1})$$

$$\Delta_{\text{AFF}} = \frac{1}{\sum_{i \in \mathcal{A}} \sum_{j,k \in \mathcal{F}} |J_{ij} J_{jk} J_{ki}|} \sum_{i \in \mathcal{A}} \sum_{j,k \in \mathcal{F}} J_{ij} J_{jk} J_{ki}, \quad (\text{D2})$$

where \mathcal{A} and \mathcal{F} denote the set of active sites and free sites. Equation (D1) is defined in terms of the triplets (i, j, k) , where i and j are in the active sites, and k is the free site, as shown in Fig. 17(a). Equation (D2) is defined for the triplets (i, j, k) , where i is in the active site, and j and k are in the free sites. For the randomly constructed genotypes, Eqs. (D1) and (D2) are zero at a sufficiently large system size. When Eqs. (D1) and (D2) defined for evolved genotypes are positive, the frustrations of the corresponding triplets are reduced through evolution.

Figure 17(b) shows the temperature dependence of the mean of the triplets of AAF and AFF. Their values increase from zero at RS1 as well as RS2, which is consistent with findings of a previous study [32]. However, compared with the results of a previous study, these values are smaller, i.e., the reduction in frustration is moderate. This moderate reduction of the frustration is caused by the existence of the two desirable patterns.

[1] R. D. Stout, C. Jiang, B. Matta, I. Tietzel, S. K. Watkins, and J. Suttles, Macrophages sequentially change their functional

phenotype in response to changes in microenvironmental influences, *J. Immunol.* **175**, 342 (2005).

- [2] A. N. Pisarchik and U. Feudel, Control of multistability, *Phys. Rep.* **540**, 167 (2014).
- [3] J. P. Changeux, The feedback control mechanisms of biosynthetic L-threonine deaminase by L-isoleucine, in *Cold Spring Harbor Symposia on Quantitative Biology* (Cold Spring Harbor Laboratory Press, 1961), pp. 313–318.
- [4] J. Monod, J. Wyman, and J. P. Changeux, On the nature of allosteric transitions: A plausible model, *J. Mol. Biol.* **12**, 88 (1965).
- [5] J.-P. Changeux, 50 years of allosteric interactions: The twists and turns of the models, *Nat. Rev. Mol. Cell Biol.* **14**, 819 (2013).
- [6] S. Fischer, K. W. Olsen, K. Nam, and M. Karplus, Unsuspected pathway of the allosteric transition in hemoglobin, *Proc. Natl. Acad. Sci. USA* **108**, 5608 (2011).
- [7] P. Maragakis and M. Karplus, Large amplitude conformational change in proteins explored with a plastic network model: Adenylate kinase, *J. Mol. Biol.* **352**, 807 (2005).
- [8] M. Karplus and Y. Q. Gao, Biomolecular motors: The F1-ATPase paradigm, *Curr. Opin. Struct. Biol.* **14**, 250 (2004).
- [9] N. I. Markevich, J. B. Hoek, and B. N. Kholodenko, Signaling switches and bistability arising from multisite phosphorylation in protein kinase cascades, *J. Cell Biol.* **164**, 353 (2004).
- [10] T. S. Hatakeyama and K. Kaneko, Transition in relaxation paths in allosteric molecules: Enzymatic kinetically constrained model, *Phys. Rev. Res.* **2**, 012005(R) (2020).
- [11] M. Stern, M. B. Pinson, and A. Murugan, Continual learning of multiple memories in mechanical networks, *Phys. Rev. X* **10**, 031044 (2020).
- [12] E. Laine, C. Goncalves, J. C. Karst, A. Lesnard, S. Rault, W.-J. Tang, T. E. Malliavin, D. Ladant, and A. Blondel, Use of allostery to identify inhibitors of calmodulin-induced activation of bacillus anthracis edema factor, *Proc. Natl. Acad. Sci. USA* **107**, 11277 (2010).
- [13] É. Laine, L. Martínez, D. Ladant, T. Malliavin, and A. Blondel, Molecular motions as a drug target: Mechanistic simulations of anthrax toxin edema factor function led to the discovery of novel allosteric inhibitors, *Toxins* **4**, 580 (2012).
- [14] A. Panjkovich and D. I. Svergun, Deciphering conformational transitions of proteins by small angle x-ray scattering and normal mode analysis, *Phys. Chem. Chem. Phys.* **18**, 5707 (2016).
- [15] A. van der Vaart, Simulation of conformational transitions, *Theor. Chem. Acc.* **116**, 183 (2006).
- [16] L. Orellana, Large-scale conformational changes and protein function: Breaking the *in silico* barrier, *Front. Mol. Biosci.* **6**, 117 (2019).
- [17] M. M. Tirion, Large amplitude elastic motions in proteins from a single-parameter, atomic analysis, *Phys. Rev. Lett.* **77**, 1905 (1996).
- [18] I. Bahar, A. R. Atilgan, and B. Erman, Direct evaluation of thermal fluctuations in proteins using a single-parameter harmonic potential, *Folding Des.* **2**, 173 (1997).
- [19] T. Haliloglu, I. Bahar, and B. Erman, Gaussian dynamics of folded proteins, *Phys. Rev. Lett.* **79**, 3090 (1997).
- [20] K. A. Henzler-Wildman, V. Thai, M. Lei, M. Ott, M. Wolf-Watz, T. Fenn, E. Pozharski, M. A. Wilson, G. A. Petsko, M. Karplus *et al.*, Intrinsic motions along an enzymatic reaction trajectory, *Nature (London)* **450**, 838 (2007).
- [21] S. Yang and B. Roux, Src kinase conformational activation: thermodynamics, pathways, and mechanisms, *PLoS Comput. Biol.* **4**, e1000047 (2008).
- [22] M. Delarue, P. Koehl, and H. Orland, *Ab initio* sampling of transition paths by conditioned Langevin dynamics, *J. Chem. Phys.* **147**, 152703 (2017).
- [23] S. Bergmann, J. Ihmels, and N. Barkai, Similarities and differences in genome-wide expression data of six organisms, *PLoS Biol.* **2**, e9 (2003).
- [24] T. S. Gunasekera, L. N. Csonka, and O. Paliy, Genome-wide transcriptional responses of *Escherichia coli* K-12 to continuous osmotic and heat stresses, *J. Bacteriol.* **190**, 3712 (2008).
- [25] S. Marguerat, A. Schmidt, S. Codlin, W. Chen, R. Aebersold, and J. Bähler, Quantitative analysis of fission yeast transcriptomes and proteomes in proliferating and quiescent cells, *Cell* **151**, 671 (2012).
- [26] Y. Matsumoto, Y. Murakami, S. Tsuru, B. Y. Ying, and T. Yomo, Growth rate-coordinated transcriptome reorganization in bacteria, *BMC Genomics* **14**, 808 (2013).
- [27] K. Kaneko, C. Furusawa, and T. Yomo, Universal relationship in gene expression changes for cells in steady-growth state, *Phys. Rev. X* **5**, 011014 (2015).
- [28] A. Schmidt, K. Kochanowski, S. Vedelaar, E. Ahrné, B. Volkmer, L. Callipo, K. Knoops, M. Bauer, R. Aebersold, and M. Heinemann, The quantitative and condition-dependent *Escherichia coli* proteome, *Nat. Biotech.* **34**, 104 (2016).
- [29] C. Furusawa and K. Kaneko, Formation of dominant mode by evolution in biological systems, *Phys. Rev. E* **97**, 042410 (2018).
- [30] Q.-Y. Tang and K. Kaneko, Long-range correlation in protein dynamics: Confirmation by structural data and normal mode analysis, *PLoS Comput. Biol.* **16**, e1007670 (2020).
- [31] A. Sakata and K. Kaneko, Dimensional reduction in evolving spin-glass model: Correlation of phenotypic responses to environmental and mutational changes, *Phys. Rev. Lett.* **124**, 218101 (2020).
- [32] A. Sakata, K. Hukushima, and K. Kaneko, Funnel landscape and mutational robustness as a result of evolution under thermal noise, *Phys. Rev. Lett.* **102**, 148101 (2009).
- [33] A. Sakata, K. Hukushima, and K. Kaneko, Statistical-mechanical study of evolution of robustness in noisy environments, *Phys. Rev. E* **80**, 051919 (2009).
- [34] A. Sakata, K. Hukushima, and K. Kaneko, Replica symmetry breaking in an adiabatic spin-glass model of adaptive evolution, *Europhys. Lett.* **99**, 68004 (2012).
- [35] S. Saito, M. Sasai, and T. Yomo, Evolution of the folding ability of proteins through functional selection, *Proc. Natl. Acad. Sci. USA* **94**, 11324 (1997).
- [36] It can be related to the inverse of the effective population size in population genetics [62,63].
- [37] J. J. Hopfield, Neural networks and physical systems with emergent collective computational abilities, *Proc. Natl. Acad. Sci. USA* **79**, 2554 (1982).
- [38] J. F. Swain and L. M. Gierasch, The changing landscape of protein allostery, *Curr. Opin. Struct. Biol.* **16**, 102 (2006).
- [39] T. Kurikawa and K. Kaneko, Multiple-timescale neural networks: Generation of history-dependent sequences and inference through autonomous bifurcations, *Front. Comput. Neurosci.* **15**, 743537 (2021).

- [40] J. Pearl, *Probabilistic Reasoning in Intelligent Systems: Networks of Plausible Inference* (Morgan Kaufmann, San Francisco, 1988).
- [41] D. Koller and N. Friedman, *Probabilistic Graphical Models: Principles and Techniques* (The MIT Press, Cambridge, 2009).
- [42] M. Mezard and A. Montanari, *Information, Physics, and Computation* (Oxford University Press, Oxford, 2009).
- [43] J. R. L. de Almeida and D. J. Thouless, Stability of the Sherrington-Kirkpatrick solution of a spin glass model, *J. Phys. A: Math. Gen.* **11**, 983 (1978).
- [44] Y. Kabashima, A CDMA multiuser detection algorithm on the basis of belief propagation, *J. Phys. A: Math. Gen.* **36**, 11111 (2003).
- [45] While the derivations of AT instability in partially connected systems, including our evolutionary model, are not straightforward, the BP algorithm is often used as a numerical method to identify the phase of partially connected systems. To prove the exact correspondence between the BP algorithm and the RSB transition a mathematical proof valid for the thermodynamic limit is required. It is considered that the correspondence holds for a wide class of models and the instability of the fixed points of BP algorithm.
- [46] H. Nishimori, *Statistical Physics of Spin Glasses and Information Processing: An Introduction* (Oxford University Press, Oxford, 2001).
- [47] M. Mézard, G. Parisi, and M. Virasoro, *Spin Glass Theory and Beyond: An Introduction to the Replica Method and Its Applications* (World Scientific Publishing Co Inc, Singapore, 1987).
- [48] T. U. Sato and K. Kaneko, Evolutionary dimension reduction in phenotypic space, *Phys. Rev. Res.* **2**, 013197 (2020).
- [49] Q.-Y. Tang and K. Kaneko, Dynamics-evolution correspondence in protein structures, *Phys. Rev. Lett.* **127**, 098103 (2021).
- [50] Y. Togashi and A. S. Mikhailov, Nonlinear relaxation dynamics in elastic networks and design principles of molecular machines, *Proc. Natl. Acad. Sci. USA* **104**, 8697 (2007).
- [51] S. Raman, N. Taylor, N. Genuth, S. Fields, and G. M. Church, Engineering allostery, *Trends Genet.* **30**, 521 (2014).
- [52] U. T. Bornscheuer and M. Pohl, Improved biocatalysts by directed evolution and rational protein design, *Curr. Opin. Chem. Biol.* **5**, 137 (2001).
- [53] I. Bahar, R. L. Jernigan, and K. A. Dill, *Protein Actions: Principles and Modeling* (Garland Science, New York, 2017).
- [54] D. J. Amit, H. Gutfreund, and H. Sompolinsky, Spin-glass models of neural networks, *Phys. Rev. A* **32**, 1007 (1985).
- [55] W. Li, J. Wang, J. Zhang, S. Takada, and W. Wang, Overcoming the bottleneck of the enzymatic cycle by steric frustration, *Phys. Rev. Lett.* **122**, 238102 (2019).
- [56] D. Wootten, A. Christopoulos, and P. M. Sexton, Emerging paradigms in GPCR allostery: Implications for drug discovery, *Nat. Rev. Drug Discovery* **12**, 630 (2013).
- [57] J. Lu, N. Byrne, J. Wang, G. Bricogne, F. K. Brown, H. R. Chobanian, S. L. Colletti, J. Di Salvo, B. Thomas-Fowlkes, Y. Guo *et al.*, Structural basis for the cooperative allosteric activation of the free fatty acid receptor GPR40, *Nat. Struct. Mol. Biol.* **24**, 570 (2017).
- [58] R. A. Frank, C. M. Titman, J. V. Pratap, B. F. Luisi, and R. N. Perham, A molecular switch and proton wire synchronize the active sites in thiamine enzymes, *Science* **306**, 872 (2004).
- [59] M. Hemery and O. Rivoire, Evolution of sparsity and modularity in a model of protein allostery, *Phys. Rev. E* **91**, 042704 (2015).
- [60] T. Tlustý, A. Libchaber, and J. P. Eckmann, Physical model of the genotype-to-phenotype map of proteins, *Phys. Rev. X* **7**, 021037 (2017).
- [61] O. Rivoire, Parsimonious evolutionary scenario for the origin of allostery and coevolution patterns in proteins, *Phys. Rev. E* **100**, 032411 (2019).
- [62] D. L. Hartl, A. G. Clark, and A. G. Clark, *Principles of Population Genetics*, 3rd ed. (Sinauer Associates, Inc. Publishers, Sunderland, 1997).
- [63] M. Kimura and T. Ohta, *Theoretical Aspects of Population Genetics (MPB-4)* (Princeton University Press, Princeton, 2020), Vol. 4.

Correction: The originally submitted manuscript contained the same image for both Fig. 15 and Fig. 16. The image for Fig. 16 has been recovered and inserted in the proper location.